Renewable and Sustainable Energy Reviews 29 (2014) 573–588

Contents lists available at ScienceDirect

Renewable and Sustainable Energy Reviews

journal homepage: www.elsevier.com/locate/rser

# The intensification technologies to water electrolysis for hydrogen production – A review

Mingyong Wang[a,*], Zhi Wang[a], Xuzhong Gong[a], Zhancheng Guo[a,b]

[a] National Engineering Laboratory for Hydrometallurgical Cleaner Production Technology, Institute of Process Engineering, Chinese Academy of Sciences, Beijing 100190, PR China
[b] State Key Laboratory of Advanced Metallurgy, University of Science and Technology Beijing, Beijing 100083, PR China

ARTICLE INFO

*Article history:*
Received 31 May 2013
Received in revised form
19 August 2013
Accepted 24 August 2013
Available online 25 September 2013

*Keywords:*
Water electrolysis
Hydrogen production
Bubble
Cell voltage

ABSTRACT

Water electrolysis derived by renewable energy such as solar energy and wind energy is a sustainable method for hydrogen production due to high purity, simple and green process. One of the challenges is to reduce energy consumption of water electrolysis for large-scale application in future. Cell voltage, an important criterion of energy consumption, consists of theoretical decomposition voltage ($U^{\theta}$), ohmic voltage drop ($i*\sum R$) and reaction overpotential ($\eta$). The kinetic and thermodynamic roots of high cell voltage are analyzed systemically in this review. During water electrolysis, bubble coverage on electrode surface and bubble dispersion in electrolyte, namely bubble effect, result in high ohmic voltage drop and large reaction overpotential. Bubble effect is one of the most key factors for high energy consumption. Based on the theoretical analysis, we summarize and divide recent intensification technologies of water electrolysis into three categories: external field, new electrolyte composition and new thermodynamic reaction system. The fundamentals and development of these intensification technologies are discussed and reviewed. Reaction overpotential and ohmic voltage drop are improved kinetically by external field or new electrolyte composition. The thermodynamic decomposition voltage of water is also reduced by new reaction systems such as solid oxide electrolysis cell (SOEC) and carbon assisted water electrolysis (CAWE).



**Contents**



* Corresponding author. Tel./fax: +86 10 82544818.
*E-mail address:* mywang@home.ipe.ac.cn (M. Wang).

1364-0321/$ - see front matter © 2013 Elsevier Ltd. All rights reserved.
http://dx.doi.org/10.1016/j.rser.2013.08.090

## 1. Introduction

Hydrogen, the clean energy carrier with the highest specific energy density, is considered as the best alternative to fossil fuel in order to ensure sustainability of energy. However, at present, 96% of hydrogen is still produced from hydrocarbon sources, such as natural gas, oil and coal (Table 1) [1]. Plenty of $CO_2$, the greenhouse gas, is released to atmosphere, and destroys the eco-environment [2–4]. Meanwhile, poisonous CO in hydrogen produced from hydrocarbon sources can deteriorate seriously the property of fuel cell which converts chemical energy of hydrogen to electric energy [5–9]. In the long run, it is not a sustainable manner to produce hydrogen from non-renewable hydrocarbon sources. Hydrogen must be produced by clean processes which use renewable sources and avoid completely the emission of carbon dioxide.

Water electrolysis for hydrogen production has many advantages such as high purity, simple process, no pollution and plenty of sources. Industrial water electrolysis cells have been established for one hundred years [10]. However, water electrolysis is only used in special cases that need hydrogen with high purity. This technology is considered as the supplement but not the alternative to hydrocarbon sources for hydrogen production in the past several decades. However, fossil fuel (coal, petroleum or natural gas) is not reliable due to the reduction of reserves and severe environmental pollution. Renewable primary energies such as solar energy, wind energy and ocean energy receive more and more attentions [11–16]. It may be an epoch-making energy revolution. The problems or disadvantages of renewable primary energy are regionalism, intermittence and unstorability, which will result in instability of power source. Hydrogen produced by water electrolysis is considered as the best energy carrier to adjust the balance between the generation of power source by renewable primary energy and energy demand for end-use [17–19]. It provides an inspiring opportunity to develop water electrolysis technology.

In future, the promising roadmap of sustainable energy is illustrated in Fig. 1. The majority of renewable energy provides power source for end-use, and excess electricity is used to electrolyze water to produce storageable hydrogen and oxygen. Then, hydrogen is transported to the regions where renewable energy is lacked, and serves to industry, traffic, electric station and household. The sustainable energy route is feasible and convenient. In United States, Xcel Energy Corporation and the U. S. Department of Energy's National Renewable Energy Laboratory (NREL) unveiled a unique facility in which electricity is produced by wind turbines. Then, water electrolysis is carried out for pure hydrogen. Intermittent wind power is converted to stored hydrogen which is used to provide power for homes and cars by fuel cell [20].

Although the prospect of the sustainable energy route in Fig. 1 is inspiring, the problems are low gas evolution rate and high energy consumption of water electrolysis. Generally, energy requirement is up to 4.5–5.0 kWh $m^{-3}H_2$ in conventional industrial electrolyzers. Therefore, it is urgent to enhance water electrolysis and reduce energy consumption in order to satisfy the requirement of sustainable hydrogen production. The aims of this paper are to analyze the roots of high energy consumption, and review the new technological advancement on kinetic and thermodynamic process intensification of conventional water electrolysis. The studies about electrode materials to catalyze gas evolution reaction and photoelectrolysis of water for hydrogen production are not reviewed.

## 2. Energy consumption of water electrolysis

Cell voltage ($U$) is an important criterion to represent energy consumption of water electrolysis. The thermodynamic decomposition voltage of water is 1.23 V. Current efficiency of hydrogen evolution reaction is up to about 100%. According to Faraday's law, the electric quantity ($Q$) to produce 1 mol $H_2$ (i.e. 22.4 L at standard condition) is 2 F. Therefore, theoretical energy consumption ($W_t$) to produce 1 $m^3$ $H_2$ is

$$W_t = UIt = UQ = 1.23 \times \left(2 \times \frac{1000}{22.4} \times 96485 \times \frac{1}{1000} \times \frac{1}{3600}\right) = 2.94\ \text{kWh/m}^3\text{H}_2 \quad (1)$$

However, no gas evolution reaction occurs until 1.65–1.7 V. Practical cell voltages of water electrolysis in industrial cell are about 1.8–2.6 V. The values are much higher than theoretical decomposition voltage of 1.23 V due to high overpotential and large ohmic voltage drop. If cell voltage is 2.0 V, practical energy consumption ($W_p$) is

$$W_p = 2 \times \left(2 \times \frac{1000}{22.4} \times 96485 \times \frac{1}{1000} \times \frac{1}{3600}\right) = 4.78\ \text{kWh/m}^3H_2 \quad (2)$$

Energy efficiency ($\eta_e$) of water electrolysis for hydrogen production is only

$$\eta_e = (2.94/4.79) \times 100\% = 61.5\% \quad (3)$$

Low energy efficiency decreases the usage efficiency of renewable primary energy.

Practical cell voltage is expressed as following:

$$U = E_a - E_c + i{*}\sum R = U^\theta + |\eta_a| + |\eta_c| + i{*}\sum R \quad (4)$$

where $E_a$ is anode potential for oxygen evolution reaction, $E_c$ cathode potential for hydrogen evolution reaction, $i$ current density, $\sum R$ total ohmic resistance, $U^\theta$ theoretical decomposition voltage, $\eta_a$ anode overpotential, $\eta_c$ cathode overpotential. According to Eq. (4), cell voltage of water electrolysis consists of theoretical decomposition voltage ($U^\theta$), reaction overpotential ($\eta$) and ohmic voltage drop ($i{*}\sum R$). Therefore, the technologies for process enhancement of water electrolysis must be focused on the reduction of $U^\theta$, $\eta$ or $i{*}\sum R$.

### 2.1. Theoretical decomposition voltage

Water electrolysis involves hydrogen evolution reaction on cathode and oxygen evolution reaction on anode, respectively. The reaction and standard equilibrium electrode potential ($E^\theta$) at 25 °C and 1 atm are written as follows:

In acid electrolyte

$$\text{Cathode} \quad 2H^+ + 2e = H_2 \qquad E_c^\theta = 0.0\ \text{V} \quad (5)$$

$$\text{Anode} \quad H_2O = 2H^+ + 1/2O_2 + 2e \quad E_a^\theta = 1.23\ \text{V} \quad (6)$$

In alkaline electrolyte

$$\text{Cathode} \quad 2H_2O + 2e = H_2 + 2OH^- \quad E_c^\theta = -0.83\ \text{V} \quad (7)$$

$$\text{Anode} \quad 2OH^- = H_2O + 1/2O_2 + 2e \quad E_a^\theta = 0.40\ \text{V} \quad (8)$$

**Acronym list**

*Symbols*

| | |
|---|---|
| $A$ | geometrical surface area of electrode ($m^2$) |
| $A_e$ | effective active area of electrode ($m^2$) |
| $D$ | change rate of cell voltage with log $G$ |
| $E_a$ | anode potential (V) |
| $E_c$ | cathode potential (V) |
| $E^\theta$ | standard equilibrium electrode potential (V) |
| $F$ | resultant force (N) |
| $g$ | gravity acceleration (9.8 $m/s^2$) |
| $\Delta G$ | energy demand (kJ) |
| $G$ | gravity coefficient |
| $i$ | current density ($A/cm^2$) |
| $i_\theta$ | real current density ($A/cm^2$) |
| $i*\sum R$ | ohmic voltage drop (V) |
| $I$ | current intensify (A) |
| $k$ | mass transfer coefficient |
| $Q$ | electric quantity (C) |
| $\sum R$ | total ohmic resistance ($\Omega$) |
| $R_b$ | bubble resistance ($\Omega$) |
| $R_c$ | circuit resistance ($\Omega$) |
| $R_e$ | electrolyte resistance ($\Omega$) |
| $R_m$ | membrane resistance ($\Omega$) |
| $R_\varepsilon$ | electrolyte resistance in the presence of bubbles ($\Omega$) |
| $S$ | supersaturation |
| $t$ | time (s) |
| $U$ | cell voltage (V) |
| $U_1$ | cell voltage of water electrolysis under normal gravity condition (V) |
| $U_G$ | cell voltage of water electrolysis under super gravity field (V) |
| $U^\theta$ | theoretical decomposition voltage (V) |
| $W_p$ | practical energy consumption (kWh/$m^3$ $H_2$) |
| $W_t$ | theoretical energy consumption (kWh/$m^3$ $H_2$) |

*Greeks*

| | |
|---|---|
| $\beta$ | contact angle (°) |
| $\gamma_{GL}$ | surface tension of gas–liquid (mN/m) |
| $\gamma_{GS}$ | surface tension of gas–solid (mN/m) |
| $\gamma_{LS}$ | surface tension of liquid–solid (mN/m) |
| $\delta$ | bubble layer thicknesses (mm) |
| $\delta_H$ | bubble layer thicknesses of cathode under normal gravity condition (mm) |
| $\delta_{HG}$ | bubble layer thicknesses of cathode under super gravity field (mm) |
| $\delta_O$ | bubble layer thicknesses of cathode under normal gravity condition (mm) |
| $\delta_{OG}$ | bubble layer thicknesses of anode under super gravity field (mm) |
| $\varepsilon$ | void fraction |
| $\Delta\eta$ | reaction overpotential reduction (V) |
| $\eta$ | reaction overpotential (V) |
| $\eta_a$ | anode overpotential (V) |
| $\eta_c$ | cathode overpotential (V) |
| $\eta_e$ | energy efficiency |
| $\eta_\theta$ | real overpotential (V) |
| $\theta$ | bubble coverage ratio |
| $v$ | detachment velocity of bubbles (m/s) |
| $\rho$ | density ($g/cm^3$) |

Total reaction is

$$H_2O = H_2 + 1/2O_2 \qquad U^\theta = 1.23\ V \tag{9}$$

Theoretical decomposition voltage ($U^\theta$) is described as following:

$$U^\theta = E_a^\theta - E_c^\theta \tag{10}$$

$U^\theta$ is a thermodynamic parameter and the value is 1.23 V at 25 °C and 1 atm. In conventional electrolytic system, $U^\theta$ is a constant at certain temperature and independent on solution composition, pH, stirring, electrode materials and so on. In the past, most of researchers are devoted to kinetically enhancing water electrolysis for hydrogen production. It is hardly focused on the reduction of thermodynamic theoretical decomposition voltage. In fact, theoretical decomposition voltage can be reduced obviously by elevating electrolytic temperature or changing reaction process to save energy consumption.

### 2.2. Overpotential

When theoretical decomposition voltage (i.e. 1.23 V) is exerted to electrolytic cell, water electrolysis is reversible kinetically. Hydrogen evolution reaction and oxygen evolution reaction hardly proceed. In order to increase the rate of water electrolysis, additional overpotentials ($\eta$) for both cathode reaction and anode reaction are indispensable to overcome energy barrier. The empirical Tafel equation is used to evaluate the relationship of overpotential $\eta$ and current density $i$:

$$\eta = a + b \log i \tag{11}$$

where both $a$ and $b$ are Tafel constants. $a$ represents the overpotential at 1 A $cm^{-2}$, and it is related to intrinsical properties and surface structure of electrode materials. According to $a$ value, metal materials as cathodes for hydrogen evolution reaction are divided into three classes:

(a) Metals with high overpotential: Cd, Tl, Hg, Pb, Zn, Sn, etc.
(b) Metals with middle overpotential: Fe, Co, Ni, Cu, Au, Ag, W etc.
(c) Metals with low overpotential: Pt, Pd

Lots of researchers were devoted to improving the catalytic activities of electrodes and reducing the overpotential of gas evolution reaction [21–34]. Considering cost and catalytic properties, Ni-based metals or alloys are considered as the best cathode materials for hydrogen evolution reaction [29–34]. However, this paper mainly focuses on technological advancement for the enhancement of convectional water electrolysis and new electrolysis processes. The development of electrode materials for gas evolution reaction has been well reviewed by Park et al. [27].

Besides electrode materials, effective active area ($A_e$) of electrode plays an important role on reaction overpotential. $A_e$ is related to surface roughness which is determined by electrode preparation [35].

**Table 1**
Annual global hydrogen production share.
Source: [1].

| Source | Bcm[a]/yr | Share (%) |
|---|---|---|
| Natural gas | 240 | 48 |
| Oil | 150 | 30 |
| Coal | 90 | 18 |
| Electrolysis | 20 | 4 |
| Total | 500 | 100 |

[a] Bcm: billion cubic meters.

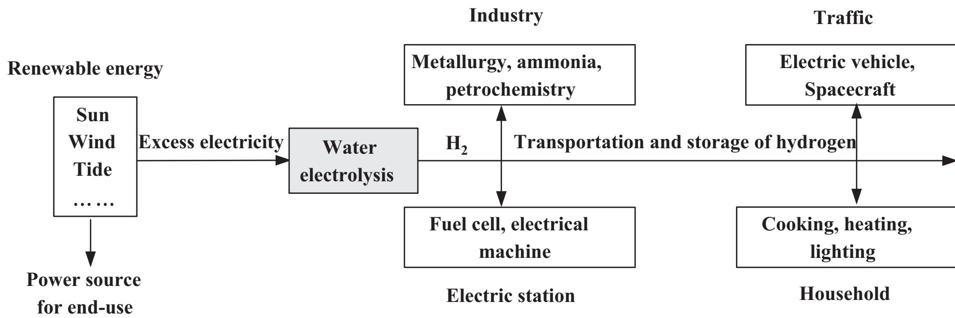



**Fig. 1.** Sustainable production and application of energy.

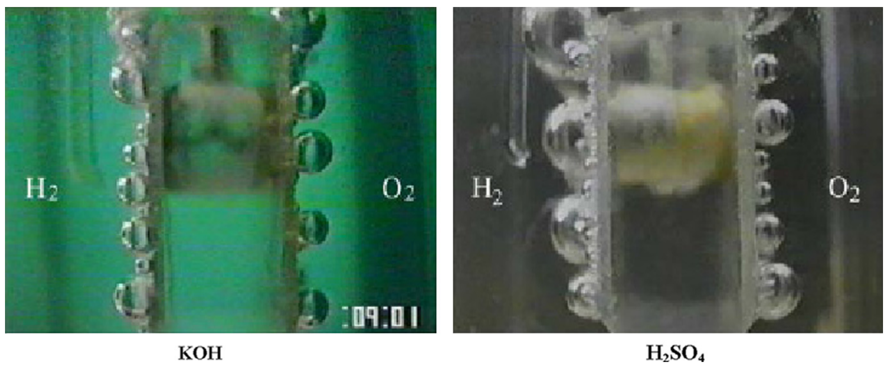



**Fig. 2.** The photograph of bubble coverage on electrode surface [39].

On the other hand, lots of bubbles are adsorbed on electrode surface during water electrolysis and act like an electric shield. Bubble coverage reduces effective active area $A_e$ for gas evolution reaction and disturbs current distribution of electrode surface. Therefore, real current density increases evidently and overpotential becomes much larger according to Tafel equation in Eq. (11), which leads to high cell voltage and energy consumption.

### 2.3. Ohmic voltage drop

Ohmic voltage drop is also a key factor leading to high energy consumption of water electrolysis. The total ohmic resistance $\sum R$ of water electrolysis is expressed as following:

$$\sum R = R_e + R_m + R_b + R_c \tag{12}$$

where $R_e$, $R_m$, $R_b$ and $R_c$ are electrolyte resistance, membrane resistance, bubble resistance and circuit resistance, respectively. $R_c$ and $R_m$ should be minimized by optimization of wire connection and production process of membrane. In electrolytic cell, both $R_c$ and $R_m$ are constants. $R_e$ is related to solution composition and electrode distance. $R_e$ decreases with increase of conductive salts such as KOH or NaOH. Generally, the concentration of KOH or NaOH is about 20%–30% for alkaline electrolyte. Further addition of conductive salt would result in the corrosion of cell and destroy of membrane. On the other hand, during water electrolysis, the dispersion of bubbles in electrolyte leads to poor conductivity and increases $R_e$. Meanwhile, lots of bubbles cover on electrode surface and disturb or shield electric field, which brings about high bubble resistance $R_b$.

## 3. Bubble effect

During water electrolysis, bubbles cannot be removed rapidly from electrolytic system, and cover on electrode surface or disperse in electrolyte. The phenomenon would lead to high overpotential and large ohmic voltage drop, namely, bubble effect. In the past, bubble effect is not taken into consideration. However, the studies about the influences of nonconducting bubbles on overpotential and ohmic voltage drop are of great interest for the optimization of water electrolysis. In this section, bubble effect is analyzed and reviewed in detail. The bubble layer adjacent to electrode consists of two layers: the first layer with bubbles covering on electrode surface and the second layer with rising bubbles dispersing in electrolyte [36].

### 3.1. Bubble coverage on electrode surface

During water electrolysis, molecular $H_2$ and $O_2$ are produced by electrochemical reaction on active sites of electrode surface and are supersaturated to form bubbles. Then, bubbles grow gradually with time. When a critical size is achieved, bubbles are disengaged from electrode surface [37]. For an efficient electrolysis process, gas released should be removed in time from active sites to increase available surface areas for gas evolution reaction [38]. However, in practical electrolytic cell, bubbles absorbed on electrode surface cover active sites during nucleation and growth. From Fig. 2, severe bubble coverage occurs on both cathode and anode. Bubbles will disturb current distribution and isolate active sites from reaction ion. Therefore, bubbles induce microconvection to push away electrolyte in a radial direction. The phenomenon leads to high reaction overpotential and large ohmic voltage drop. Aldas [38] also confirmed by numerical investigation that bubble layer adsorbed on electrode surface decreases gas evolution rate seriously.

Theoretically, current density for gas evolution reaction is

$$i = \frac{I}{A} \tag{13}$$

where $I$ is current intensify, $A$ is the geometrical surface area of electrode. Thus, reaction overpotential should be written as following according to Tafel equation:

$$\eta = a + b\log i = a + b\log\frac{I}{A} \tag{14}$$

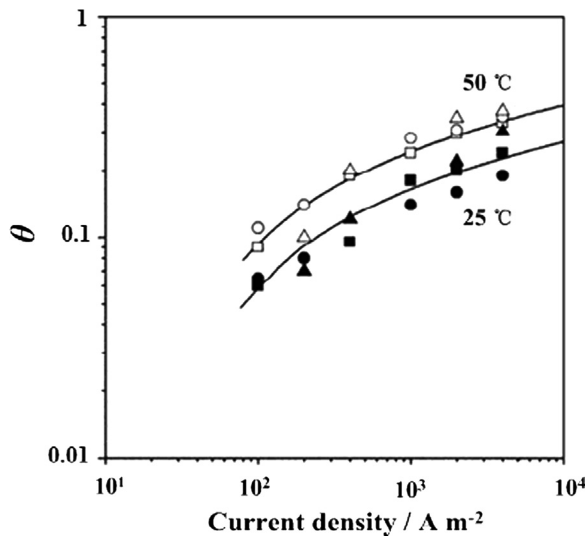



**Fig. 3.** Bubble coverage ratio $\theta$ as function of current density [40].

However, bubble coverage reduces efficient active area of electrode. Real current density ($i_\theta$) and overpotential ($\eta_\theta$) are

$$i_\theta = \frac{I}{A(1-\theta)} \tag{15}$$

$$\eta_\theta = a + b\log i_\theta = a + b\log\frac{I}{A(1-\theta)} = a + b\log\frac{I}{A} + b\log\frac{1}{(1-\theta)} = \eta + b\log\left(\frac{1}{1-\theta}\right) \tag{16}$$

where $\theta$ is bubble coverage ratio on electrode surface, $0<\theta<1$. Krenz [40] observed that $\theta$ increased with current density and temperature. An increase of about 50% in bubble coverage was observed with the increase of temperature from 25 °C to 50 °C (Fig. 3). Balzer and Vogt [41] also reported that the surface coverage ratios were 0.2 at 140 mA cm$^{-2}$ and 0.22 at 200 mA cm$^{-2}$, respectively. Severe bubble coverage reduces efficient active area of electrode. Therefore, $i_\theta$ becomes larger than $i$, and reaction overpotential is also higher according to Tafel equation. Dukovic and Tobias [42] investigated the effect of bubbles by using hexagonally ordered dielectric spheres as model. They concluded that the increase of overpotential was the dominant voltage effect in Tafel kinetic regime. It was reported that in a well-designed industrial cell, bubble coverage incurs large overpotential, e.g. about 0.4 V at a current density of 300 mA cm$^{-2}$ [43].

On the other hand, lots of nonconductive bubbles cover electrode surface and form an insulating layer. Qian et al. [44] reported that ohmic resistance was proportional to bubble coverage ratio. Kiuchi et al. [37] measured bubble layer thickness under microgravity and found that ohmic resistance of bubble froth increased with bubble layer thickness. Based on above discussion, bubble coverage on electrode surface leads to high reaction overpotential and ohmic voltage drop.

### 3.2. Bubble dispersion in electrolyte

When the diameter of bubbles is up to a critical value, bubbles detach from electrode surface into electrolyte. The second bubble layer is formed in vicinity of electrode surface. The relative motion between gas phase and liquid phase occurs and the moving track of bubbles is shown in Fig. 4. Bubbles ascend along the $z$ axes direction due to buoyancy and density difference between gas and liquid. Meanwhile, bubbles also move along the $y$ axes direction due to concentration difference of gas in electrolyte. Therefore, real moving track of bubbles is determined by the resultant force $F$. Bubbles overflow in the top of cell. Finally, a bubble froth layer is formed due to the low detachment rate of bubbles from electrolyte. The thickness of bubble froth layer increases as a function of electrolyte height (Fig. 4). Matsushima et al. [46] observed by high-speed camera that bubbles began to detach from electrode surface within 0.15 s. At the top part, bubble curtain swirled and formed a stable bubble layer after 0.5 s (Fig. 5).

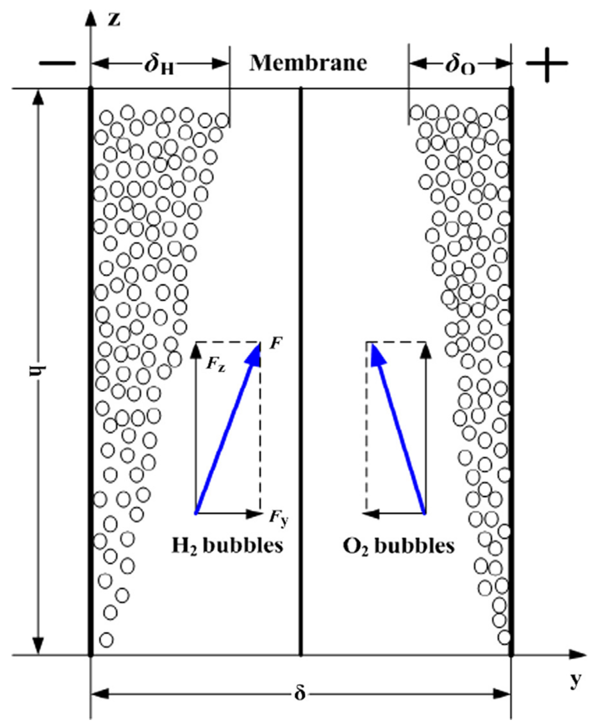



**Fig. 4.** Schematic sketch of bubble layer formed in the vicinity of electrode surface [45].

Generally, the dispersion of bubbles in electrolyte and the conductivity of electrolyte are represented and affected by void fraction ($\varepsilon$). $\varepsilon$ is related to solution composition, pressure, current density, bubble size, bubble layer thickness, electrode space, and so on. Void fraction in bubble froth layer is estimated by Bruggeman equation [47]

$$\frac{R_\varepsilon}{R_e} = (1-\varepsilon)^{-3/2} \tag{17}$$

where $R_\varepsilon$ is electrolyte resistance in the presence of bubbles, and $R_e$ is electrolyte resistance. Experimental studies are usually focused on the relationship between effective conductivity of electrolyte and void fraction of gas phase. Mandin et al. [48] examined the accumulation of bubbles and found that void fraction was larger in higher parts of electrodes, which brings about higher cell voltage. Janssen [49] used spherical glass beads as model and studied the effect of bubble dispersion on ohmic resistance. It was found that effective ohmic resistance of electrolyte was well described by Bruggeman equation. In practical water electrolysis system, it is difficult to measure directly ohmic resistance of bubble dispersion zone due to rapid bubble movement. In view of the slow convection velocity under microgravity, Matsushima et al. [46] studied the effect of bubble void fraction on ohmic resistance by applying current interrupt method. They found that $\varepsilon$ values were about 0.5 and 0.4 in the vicinity of oxygen evolution electrode and hydrogen evolution electrode, respectively. High void fraction brings about large electrolyte resistance and high ohmic voltage drop due to nonconductive bubble layers.

Low detachment and spillover rate of bubbles from electrode surface and electrolyte result in severe bubble effect, i.e. large reaction overpotential and high ohmic voltage drop. It is the main root of high energy consumption of water electrolysis. Therefore, the minimization

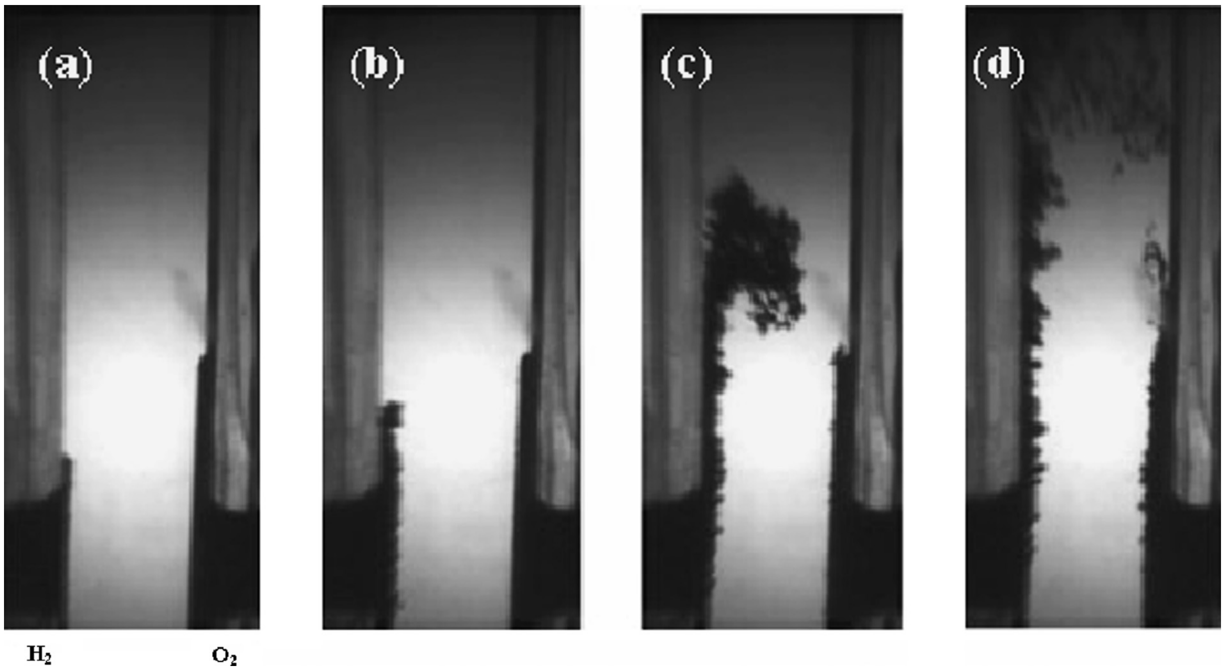



**Fig. 5.** Transient of gas evolution behavior [46]. (a) 0.05 s, (b) 0.15 s, (c) 0.30 s and (d) 0.5 s.

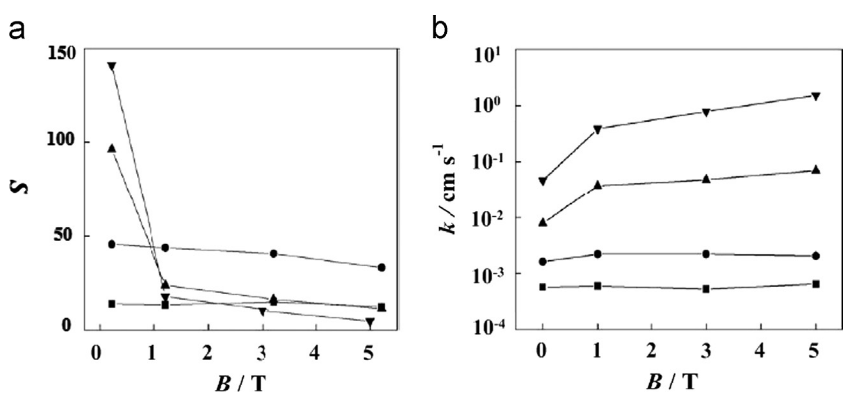



**Fig. 6.** Supersolubility, *S*, (a) and mass transfer coefficient, *k*, (b) of dissolved $H_2$ gas as function of magnetic field intensity, *B* [58]. ■ 1 mA cm$^{-2}$, ● 10 mA cm$^{-2}$, ▲ 100 mA cm$^{-2}$ and ▼ 1000 mA cm$^{-2}$.

of bubble effect is an important issue to enhance water electrolysis and save energy.

## 4. Enhanced technology by external field

The combined negative effect of bubble coverage on electrode surface and bubble dispersion in electrolyte increases inevitably energy consumption of water electrolysis. Therefore, it is beneficial to accelerate the detachment of bubbles from electrolytic system in order to enhance water electrolysis. For instance, (1) more effective disengagement of bubbles from electrode and membrane surface to decrease ohmic voltage drop and reaction overpotential; (2) more effective spillover of bubbles from electrolyte to reduce electrolyte resistance; (3) rapid removal of bubbles from electrode surface to improve mass transfer [50]. Electrolyte flow is usually applied to promote bubble separation from electrolyte in commercial water electrolysis cell [51,52]. Unfortunately, high ohmic voltage drop and cell voltage can be only eliminated to a limited extent [40]. Recently, many researchers exert external fields to water electrolysis and cell voltage is reduced remarkably.

### 4.1. Magnetic field

The enhancement effect of magnetic field on electrochemical reaction is focused due to a magnetohydrodynamic (MHD) convection induced by Lorenz force [53–55]. Iida et al. [56] superimposed a high magnetic field of 5 T to water electrolysis. Large reduction of cell voltage was achieved, especially in alkaline solution and at high current density. Lin et al. [57] found that magnetic effect was more significant by shortening inter-electrode distance. Ferromagnetism such as nickel is better cathode material than paramagnetism (platinum) and diamagnetism (graphite) under magnetic field. For nickel electrode, the increasing ratio of current density was about 14.6% with an inter-electrode distance of 2 mm and cell voltage of 4 V. The improvement of water electrolysis process under magnetic field may be ascribed to the enhancement of convection and bubble disengagement.

Matsushima et al. [58] measured supersaturation (*S*) in the interface of electrode-electrolyte and mass transfer coefficient (*k*) of dissolved $H_2$ by current interrupter method. As shown in Fig. 6, *S* value decreases and *k* value increases as a function of magnetic field intensity, especially at higher current density. Magnetic field promotes mass transfer of dissolved $H_2$ to release supersaturation in the vicinity

of electrode. It is well known that gas evolution reaction occurs in the three-phase interface of gas–liquid–solid. Therefore, the nucleation, growth and detachment of bubbles are affected by surface tension of gas–liquid ($\gamma_{GL}$), gas–solid ($\gamma_{GS}$) and liquid–solid ($\gamma_{LS}$) interface (Fig. 7). When magnetic field is perpendicular to electrode, a drag force is induced to increase contact angle ($\beta$) and promotes the detachment of bubbles from electrode surface [59]. Therefore, detachment velocity ($\nu$) of bubbles is accelerated due to MHD convection rather than natural convection, especially at larger magnetic field intensity than 1 T (Fig. 8a). The rising detachment velocity reduces residential time of bubbles on electrode surface and diminishes bubble coverage (Fig. 8b) [60]. Similar phenomenon was also demonstrated by Koza et al. [61]. According to Eq. (16), real overpotential ($\eta_\theta$) for gas evolution reaction is reduced due to lower bubble coverage under magnetic field. Meanwhile, a reduction of ohmic voltage drop from insulating bubble layer on electrode surface is achieved.

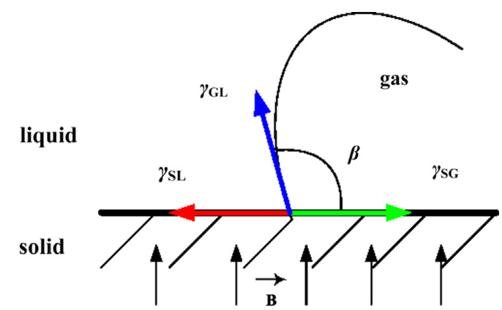



**Fig. 7.** Surface tensions between gas–liquid–solid interfaces [59].

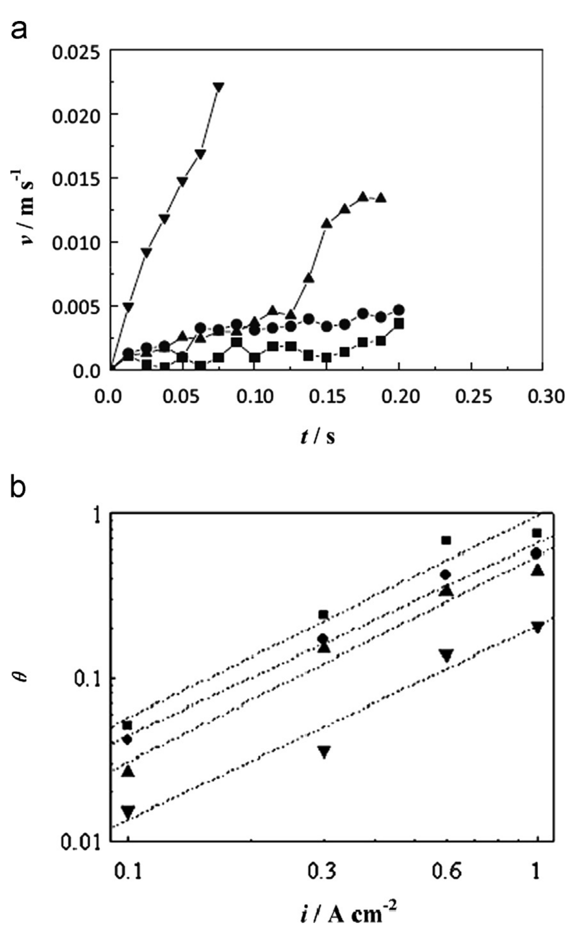



**Fig. 8.** The average rising velocity (a) and surface coverage (b) of oxygen bubbles on FTO glass electrode [60]. $B=0$ T (■), 0.5 T (●), 1 T (▲) and 5 T (▼).

On the other hand, bubbles dispersed in electrolyte in the vicinity of electrode bring about large electrolyte resistance and high ohmic voltage drop. The negative effect of bubble dispersion becomes more serious with the increase of $\varepsilon$ value. Matsushima et al. [46] found that average bubble layer thicknesses ($\delta$) on both cathode and anode were reduced by magnetic field (Fig. 9). It means that magnetic field promotes the rapid disengagement of bubbles from electrolyte. Furthermore, void fraction was calculated and shown in Fig. 10. $\varepsilon$ values decreased from 0.40 to 0.28 for hydrogen bubbles and from 0.48 to 0.41 for oxygen bubbles, respectively [46]. Lower void fraction increases the conductivity of electrolyte and decreases ohmic voltage drop.

Magnetic field decreases bubble coverage on electrode surface and void fraction of dispersed bubbles in electrolyte. Therefore, ohmic voltage drop and reaction overpotential are reduced obviously in the presence of magnetic field, which leads to lower cell voltage of water electrolysis.

### 4.2. Ultrasonic field

Ultrasonic field is a powerful tool to promote mass transfer and enhance electrochemical reaction based on cavitations effect. Li et al. [50] studied the effect of ultrasonic field on water electrolysis in alkaline solution. The results indicated that cell voltage was decreased obviously due to the application of ultrasonic field, especially at higher current density and lower electrolyte concentration. At constant current density, cell voltage reduction under ultrasonic field decreased with the increase of NaOH concentration. The efficiency of $H_2$ production was increased in the range of 5–18% at higher current density under ultrasonic field and energy saving was up to 10–25% (Fig. 11).

The combination effect of ultrasonic field and polyvinylidene fluoride-grafted 2-methacrylic acid 3-(bis-carboxymethylamino)-2-hydroxyl-propylester bipolar membrane (PVDF-g-G-1 BM) for $H_2$ production was further studied [62]. As shown in Fig. 12, $H_2$ production efficiency for electrolytic cell with ultrasonic field was higher than that without ultrasonic field. Energy savings of $H_2$ production using PVDF-g-G-1 BM as membrane were up to 15–20% and 8–12% for cell operated with and without ultrasonic field, respectively.

Under ultrasonic field, lots of cavitation bubbles are produced due to cavitation effect. During water electrolysis, gas evolved on electrode combines with cavitation bubbles or is used as nucleus to form cavitation bubbles. Therefore, fine bubbles are formed more easily under ultrasonic field. With the periodical collapse of cavitation bubbles, the disengagement of hydrogen or oxygen bubbles from electrode surface and electrolyte is accelerated due to violent agitation effect. Reaction overpotential and ohmic voltage drop are reduced by ultrasonic field.

### 4.3. Super gravity field

Bubble effect due to low disengagement rate of bubbles from electrolytic cell is a significant issue for high cell voltage of water electrolysis. It is well known that the motion of bubbles from electrode surface, membrane and electrolyte is controlled by interphase buoyancy term, $\Delta\rho g$ [43]. Buoyancy is the actual driving force for bubble disengagement. During water electrolysis, bubbles move along buoyancy direction. Therefore, if an external force is exerted on bubbles along buoyancy direction, the disengagement of bubbles is promoted more effectively.

Super gravity field with high gravity acceleration ($g$) is used widely to enhance phase separation [63–66]. In the past decade, it is also applied to intensify electrochemical reaction including electrodeposition, chlor-alkali electrolysis and water electrolysis [67–74]. Under super gravity field, heavy phase (such as electrolyte) moves along

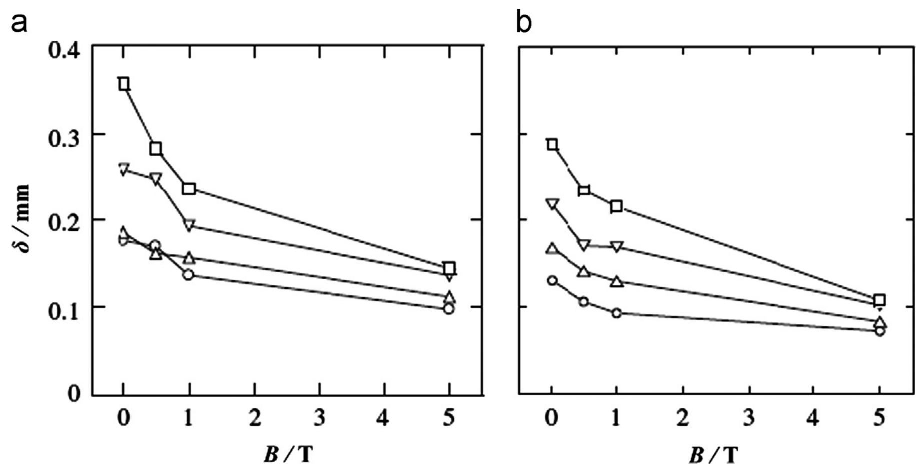



**Fig. 9.** The effect of magnetic field on bubble layer thickness ($\delta$) of hydrogen (a) and oxygen (b) [46].

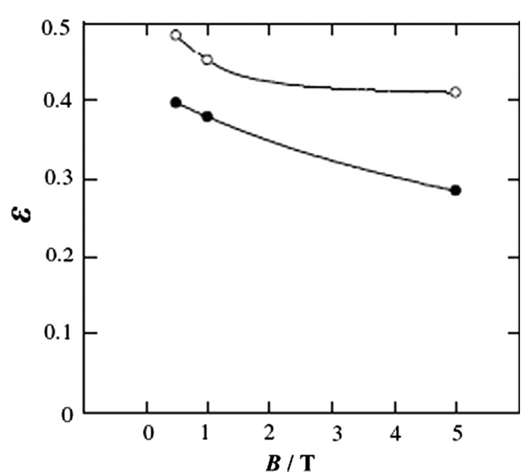



**Fig. 10.** Void fraction ($\varepsilon$) of bubble layer on hydrogen (filled squares) and oxygen (empty circles) evolution electrode in various magnetic fields [46].

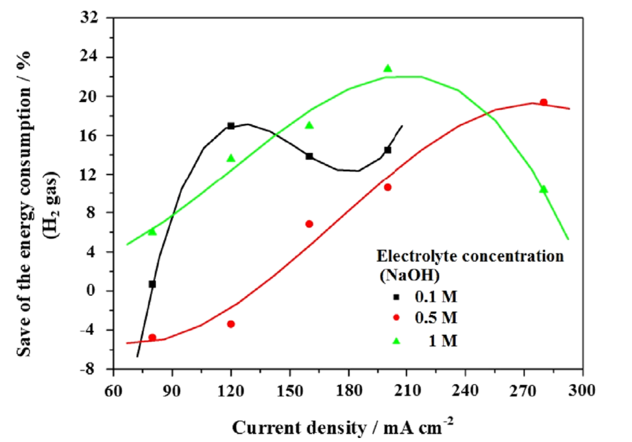



**Fig. 11.** The energy saving of $H_2$ production in the presence of the ultrasonic field in 0.1, 0.5 and 1.0 M NaOH at constant current density [50].

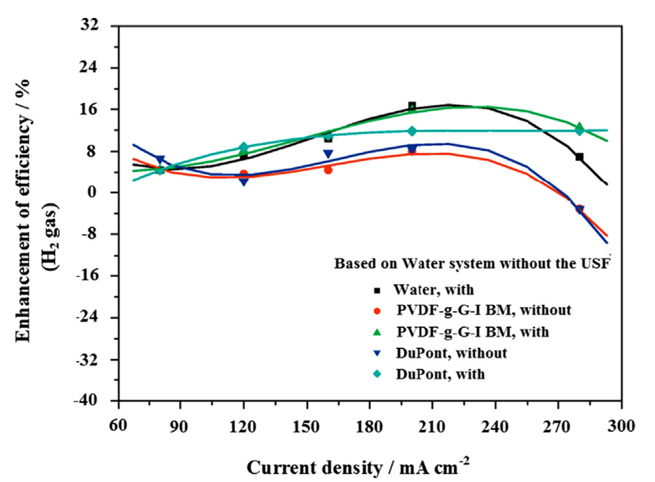



**Fig. 12.** The effect of the PCDG-g-G-I BM and ultrasonic field (USF) on the $H_2$ production efficiency (compared to water without ultrasonic field) [62].

gravity direction, while light phase (such as bubbles) moves along counter direction, i.e. buoyancy direction. Therefore, high gravity acceleration can increase interphase slip velocity and intensity gas–liquid or gas–solid phase separation. During water electrolysis, bubble coverage on electrode surface and bubble dispersion in electrolyte can be weakened in the presence of super gravity field. Therefore, both reaction overpotential and ohmic voltage drop are reduced, which results in lower cell voltage and energy consumption.

Cheng et al. [75] firstly demonstrated that super gravity field provided a powerful method for process intensification of water electrolysis. A cell voltage reduction of about 0.7 V at 3 kA $m^{-2}$ was achieved under a relative acceleration of 190 g, compared to that under normal gravity condition. Similar results were also obtained in our lab [76]. The relationship between cell voltage of water electrolysis under super gravity field ($U_G$) and gravity coefficient ($G$) is expressed using the general formula [75,76]:

$$U_G = D \log G + U_1 \tag{18}$$

where $U_1$ is cell voltage under normal gravity condition ($G=1$). $D$, a negative number and constant at certain current density, is the change rate of cell voltage with log $G$. The absolute value of $\beta$ increases as a function of current density ($i$) [76]. That is, the higher current density for water electrolysis is, the larger the effect of super gravity field on cell voltage reduction is. The maximum percent of energy saving is up to about 17% [76]. Furthermore, it was found that cell voltage reduction was mainly ascribed to ohmic voltage drop reduction compared to reaction overpotential reduction ($\Delta\eta$), especially at higher current density and gravity acceleration (Fig. 13).

Obviously, cell voltage reduction originates from rapid disengagement of bubbles from electrode surface and electrolyte. We observed bubble coverage on electrode surface during water electrolysis [77]. Lots of bubbles with diameter of about 200 μm were adsorbed on

electrode surface under normal gravity condition (Fig. 14A). However, little bubbles were observed under super gravity field (Fig. 14B), and the movement of bubbles was almost invisible. It means that residential time of bubbles on electrode surface is shortened. Super gravity field promotes the disengagement of bubbles and decreases bubble coverage on electrode surface. Therefore, reaction overpotential and ohmic voltage drop are reduced due to high active area. The relative values of critical volume and buoyancy force of bubbles under normal gravity condition and super gravity field ($G=200$) were calculated based on nucleation theory. Under super gravity field, critical volume of bubbles was only 0.094 times, while the buoyancy force was 18.8 times compared to those under normal gravity condition [77]. Mat and Aldas [78] also demonstrated that gas evolution rate was enhanced with lower bubble diameters due to higher fluid velocity. Larger buoyancy force and smaller bubble volume under super gravity field are favorable for rapid separation of bubbles from electrolytic cell. As a result, bubble layer thicknesses ($\delta_{HG}$ and $\delta_{OG}$) in the vicinity of both cathode and anode under super gravity field (Fig. 15) are smaller than those ($\delta_H$ and $\delta_O$) under normal gravity condition in Fig. 4. Therefore, electrolyte resistance and ohmic voltage drop due to bubble dispersion in electrolyte are reduced by super gravity field. Although energy saving of water electrolysis under super gravity field is examined quantitatively, the enhanced mechanism is only discussed qualitatively based on bubble separation. Further understanding into the enhanced effect of super gravity field on water electrolysis need to be analyzed quantitatively, such as void fraction, bubble coverage, supersolubility, etc.

Energy saving of water electrolysis is achieved under super gravity field, but the obtainment of stable super gravity field is an urgent issue. Meanwhile, the energy needed to obtain super gravity field must be lower than the saved energy in order to meet application purpose. Cheng et al. [75] estimated that potential energy saving was up to 30 kW in a 100 kA electrolytic cell, while the energy was only 2 kW for super gravity field. In order to maximize energy saving of water electrolysis under super gravity field, two novel strategies may be considered. Firstly, based on the fluctuation of wind power, excess electricity at peak period is supplied to electrolyze water for hydrogen production. The wind turbine blades are constructed to cell for water electrolysis. Super gravity field is obtained in electrolytic cell by the rotation of blades. Therefore, the energy for super gravity field can be neglected. Wind power is transformed adequately to electric power and hydrogen. Secondly, the bodies of transportation vehicles (such as car, bus et al.) are covered by thin film solar cells to generate electric power. Super gravity field is obtained by the rotation of wheels which are constructed to electrolytic cell. Hydrogen from water electrolysis is transformed into electric power by fuel cell to drive vehicles. However, the conceptions are very novel and the feasibility need be still verified.

External fields promote the disengagement of bubbles from electrolytic cell and enhance mass transfer. Therefore, water electrolysis is kinetically intensified and energy for hydrogen production is saved. However, the cost and energy to construct

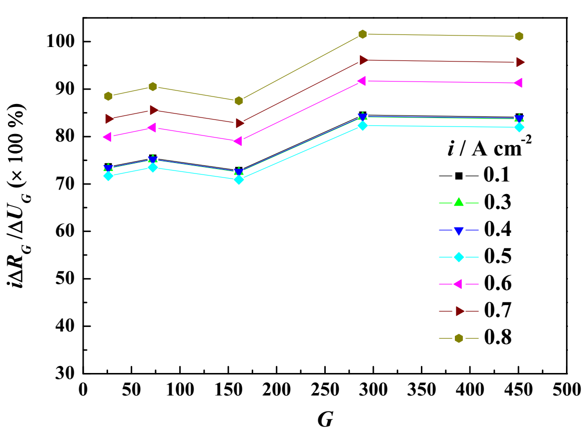



**Fig. 13.** The share of ohmic voltage drop reduction ($i\Delta R_G$) in cell voltage reduction ($\Delta U_G$) [76].

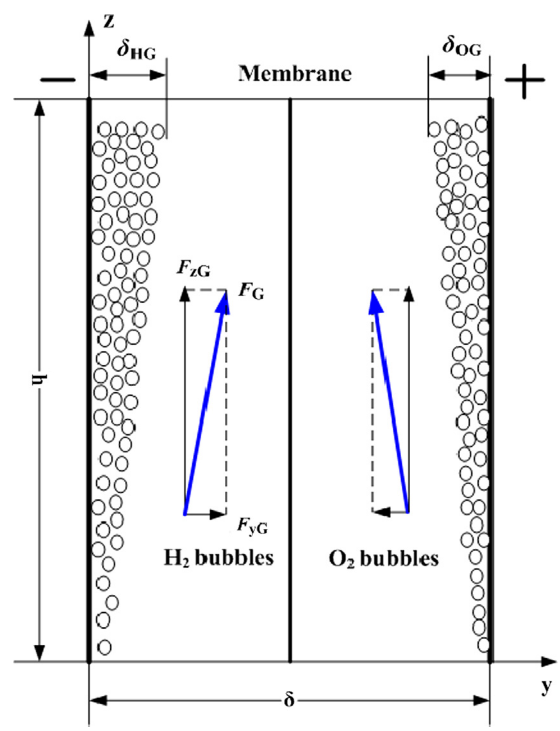



**Fig. 15.** Schematic sketch of bubbles layer formed in the vicinity of electrode surface under super gravity field.

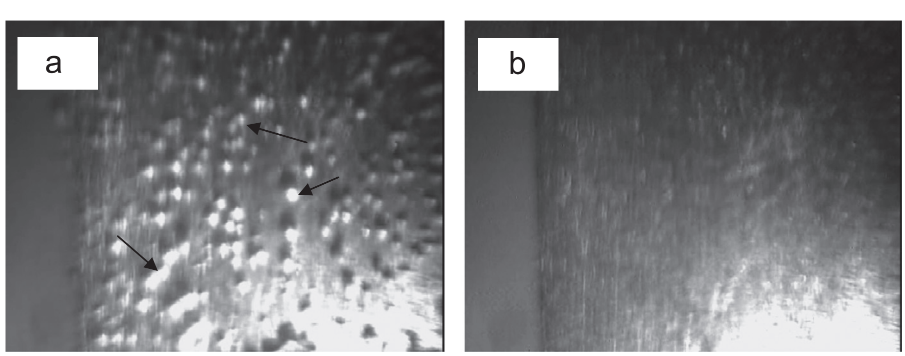



**Fig. 14.** The photograph of electrode surface during hydrogen bubble evolution process under (a) normal gravity condition ($G=1$) and (b) super gravity field ($G=101$) [77].

and drive the equipments for external fields must be considered comprehensively.

## 5. New electrolyte composition

### 5.1. Additives in electrolyte

In order to reduce energy consumption of water electrolysis, most of studies are focused on electrode materials, process intensification and new electrolytic cell. However, fewer studies are devoted to electrolyte which is usually KOH, NaOH or $H_2SO_4$ solution for conventional water electrolysis. Adding activating compounds in situ into electrolyte may obtain highly active electrodes which possess excellent stability.

In the past decade, ionic activators added in electrolyte have attracted more and more attentions. Most of ionic activators for hydrogen evolution reaction are composed of ethylenediamine-based metal chloride complex ($[M(en)_3]Cl_x$, M=Co, Ni, et al.) and $Na_2MoO_4$ or $Na_2WO_4$ [79–86]. During electrolysis, metal composites are electrodeposited in situ on cathode surface and exhibit better catalytic activity for hydrogen evolution reaction than those electrodeposited ex-situ. Stojic et al. [84] added tris(ethylenediamine)cobalt (III) chloride complex ($[Co(en)_3]Cl_3$) or tris(trimethylenediamine) cobalt(III) chloride complex ($[Co(tn)_3]Cl_3$) into KOH solution to catalyze hydrogen evolution reaction. Energy saving is up to 10%, compared to that of non-activated electrolyte. The reason is ascribed to double electrocatalytic effect of metal film with high surface area on electrode surface and organic complex ligands in electrolyte. Nikolic et al. [85] used the mixture of sodium tungstate and $[Co(en)_3]Cl_3$ as ionic activator and the reduction of energy requirement is about 15%. The enhancement mechanism of water electrolysis is the synergetic effect of Co and W on electrode surface due to high specific surface area (Fig. 16). Tasic et al. [86] used $Na_2MoO_4$ and $[Ni(en)_3]Cl_2$ as ionic activators and demonstrated further that the reasons of excellent catalytic properties are not only high surface area, but also true catalytic effect.

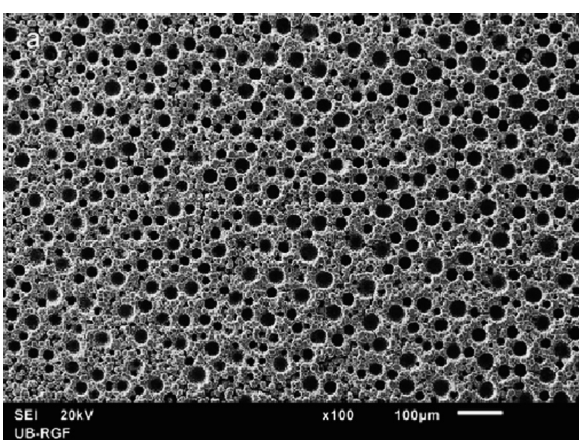



**Fig. 16.** SEM images of cathode after electrolytic process at current density of 30 mA cm$^{-2}$ for 5 h [85].

Besides ionic activators, Wei et al. [87] added hexadecyltrimethylammonium bromide (HTMAB), cationic surfactant, into $H_2SO_4$ electrolyte to enhance water electrolysis. They found that HTMAB inhibited hydrogen evolution reaction and promoted oxygen evolution reaction. However, the increase of oxygen evolution rate was larger than the reduction of hydrogen evolution rate. The similar effect of surfactant on oxygen evolution reaction was also reported in other papers [88,89]. The reason is ascribed to the enhancement of $H_2O_2$ production rate. Therefore, it is possible to obtain $H_2O_2$ rather than $O_2$ on anode during water electrolysis in acidic electrolyte [87].

The idea that adds catalytic compounds into electrolyte in situ to enhance gas evolution reaction is an efficient method due to low cost and simple operation. The redox reaction of organic compounds on electrode surface must be avoided. Surfactants which adjust the wettability of electrodes to accelerate the disengagement of bubbles should be also developed and applied.

### 5.2. Ionic liquid/water electrolyte

In conventional water electrolysis, corrosive reagents such as NaOH, KOH and $H_2SO_4$, are usually used as conductive salts. Metal electrodes as catalysts suffer from serious destruction in corrosive electrolyte and lose catalytic activity. Therefore, low stability of metal electrodes is another major problem of water electrolysis.

Ionic liquids exhibit good conductivity and are chemically inert to metal electrodes. Souza et al. [90] used $BMIBF_4$ as conductive electrolyte for hydrogen production by water electrolysis. The catalytic activities of electrodes are not affected. The mechanism of hydrogen evolution reaction was consistent on gold, molybdenum, nickel, titanium and platinum electrodes [91]. Furthermore, electrode materials, types of ionic liquid and concentration in water were optimized [92,93]. The best efficiency of about 99% was obtained in the solution of 10 vol% $BMIBF_4$ and 90 vol% water [90]. Considering efficiency, cost and stability of hydrogen production, Mo electrode was extremely attractive, even excelled Pt electrode [93]. Pool et al. [94] designed a molecular electrocatalyst ($[Ni(P_2N_2)_2](BF_4)_2$) as medium in highly acidic ionic liquid/water electrolyte to promote the reduction of protons to $H_2$. Catalytic cycle for hydrogen production was shown in Fig. 17. Hydrogen evolution reaction was enhanced obviously due to reduction of overpotential, compared to that in acetonitrile with dimethylformamidium trifuoromethanesulfonate and water. However, the viscosity of ionic liquid is large, which affects negatively the

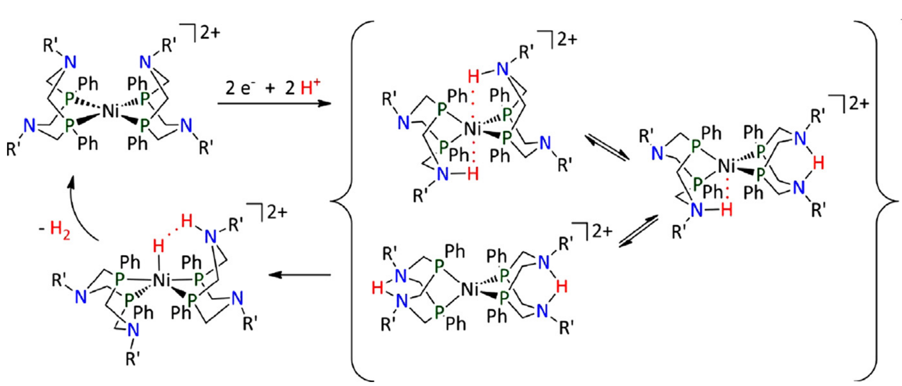



**Fig. 17.** Catalytic cycle for hydrogen production mediated by complexes [94].

transportation rate of ions. Current density, i.e. hydrogen production rate, is also low in ionic liquid/water system [95].

## 6. New system for water electrolysis

External fields and additives can enhance kinetically water electrolysis for hydrogen production. Ohmic voltage drop ($i*\sum R$) and reaction overpotential ($\eta$) are decreased due to more rapid bubble disengagement from electrolytic cell and higher gas evolution rate. However, thermodynamical decomposition voltage ($U^{\theta}$) is not changed. Thus, it is a promising method by elevating temperature or changing reaction route to diminish theoretical decomposition voltage of water for maximizing energy saving.

### *6.1. Solid oxide electrolysis cell*

The thermodynamics of water electrolysis was calculated by HSC software and shown in Fig. 18. The values of electric energy demand ($\Delta G$) and theoretical decomposition voltage ($U^{\theta}$) are 474 kJ mol$^{-1}$ and 1.23 V at 25 °C and 1 atm, respectively. Decomposition process of water is an endothermic reaction. Electric energy demand and decomposition voltage decrease with the increase of temperature. For example, at 900 °C, electric energy demand and decomposition voltage of water (i.e. steam) are 366 kJ mol$^{-1}$ and 0.95 V, respectively. Theoretical energy saving is up to 23%, compared to that at 25 °C. Meanwhile, overpotentials and ohmic voltage drop are also decreased obviously at high temperature. The facility for water steam electrolysis is called as solid oxide electrolysis cell (SOEC) which is the reverse process of solid oxide fuel cell (SOFC) [96]. The principle of SOEC is illustrated in Fig. 19. Cathode for hydrogen evolution reaction and anode for oxygen evolution reaction are isolated by solid electrolyte. At higher temperature (600–1000 °C), $H_2O$ is decomposed to $H_2$ and $O^{2-}$ on cathode. Then, $O^{2-}$ is transported through solid electrolyte to anode and oxidized to $O_2$. The conventional solid electrolyte is $ZrO_2$ doped with $Y_2O_3$ (YSZ) which possesses excellent conductivity and stability [97,98]. In addition, Scandia doped $ZrO_2$, ceria-based and $LaGaO_3$-based materials are also used as solid electrolyte [99–102]. In order to improve diffusion and transportation rate of gas, electrode materials are usually porous. Feasible electrode materials must exhibit high catalytic activity and be difficult to be degraded. The most common cathode material for hydrogen evolution reaction is Ni/YSZ [103–106]. Other materials such as samaria doped ceria (SDC), titanate/ceria and $(La_{0.75}Sr_{0.25})_{0.95}Mn_{0.5}Cr_{0.5}O_3$(LSCM)/YSZ are also reported [107–109]. Lanthanum strontium manganite (LSM)–YSZ, also used in SOFC, is the best candidate for anode materials [110–112]. The alternatives are $Ce_{0.6}Gd_{0.4}O_{1.8}$ (CG4) [113], $Ln_2NiO_{4+\gamma}$ (Ln = La, Nd, Pr) [114,115]. The key materials for solid electrolyte, cathode and anode

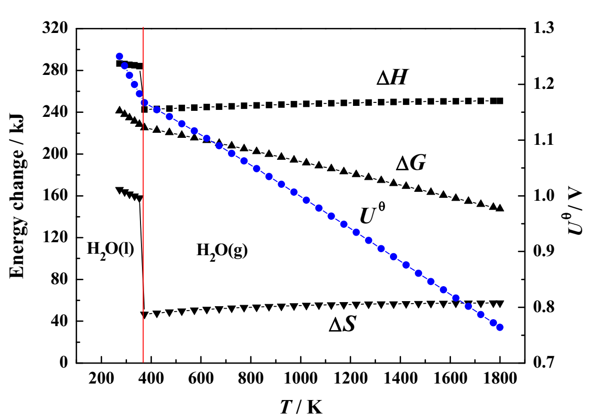



**Fig. 18.** The thermodynamics of water electrolysis at various temperatures.

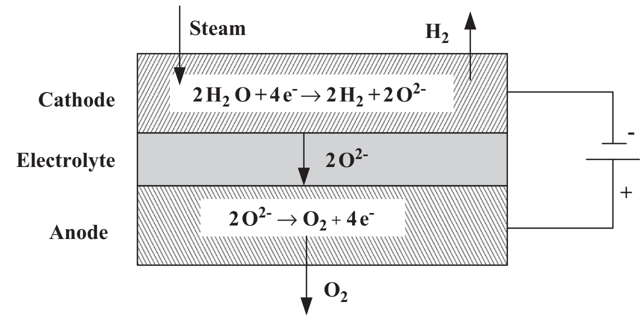



**Fig. 19.** The illustration of solid oxide electrolysis cell (SOEC).

have been well reviewed in previous papers [96,116,117]. The common SOEC stacks are tubular configuration with higher mechanical strength and planar configuration with better manufacturability [116]. Hino et al. [118] found that planar SOEC stack is quite advantageous due to more uniform distribution of gas species and easier mass production.

Udagawa et al. [119] examined steady state performances of SOEC at current density of 7000 A m$^{-2}$ and cathode inlet steam temperature of 850 °C. Cell voltage is only 1.30 V, which corresponds to an electricity consumption of about 3.1 kWh per normal m$^3$ of $H_2$. Joel et al. [120] found that cell voltage reduction by natural gas assistant SOEC was up to 1 V, compared to convectional water electrolysis. The lower energy consumption and higher efficiency of SOEC attract more and more attentions. However, a noticeable issue is energy source that heats steam to operation temperature (600–1000 °C). Nuclear power produces heat and electricity simultaneously, and is coupled with SOEC [121]. This technology for hydrogen production is listed as the top ten progresses of science and technology by Chinese Academy of Sciences (CAS) in 2004 year. Zhang et al. [122] estimated the efficiencies of SOEC coupled with nuclear reactors. At operating temperature of 850 °C, overall thermal-to-hydrogen conversion efficiencies ($\eta_{overall}$) are from 27% to 55%, when the outlet temperatures of steam are from 250 to 800 °C. Utgikar and Thiesen [123] carried out life cycle assessment of SOEC coupled with nuclear energy. The results indicated that SOEC exhibited higher energy efficiency over conventional alkaline electrolysis due to lower cell voltage and electrical energy demand. The global warming potential (GWP) and acidification potential (AP) of this system are only one-sixth and one-third of those for the hydrogen production by steam reforming of natural gas, respectively. The environmental impacts are comparable to hydrogen production from conventional water electrolysis powered by wind- or hydro-electricity. Alternative energy sources to heat steam is waste heats from chemical, metallurgical and thermal power generation industries [124,125]. This route recovers waste heats to preheat steam to operating temperature and possesses better economy. In addition, solar energy and geothermal heat are also considered as heat sources for SOEC [126].

SOEC shows higher energy efficiency for hydrogen production, compared to alkaline or proton exchange membrane (PEM) water electrolysis. Some key materials and equipments need to be improved for practical application in large scale. For example, stacks including electrode materials, solid electrolyte and sealing materials must be run stably at high temperature and humidity. Heat exchanger should preheat steam to operating temperature more efficiently and quickly. Another challenge for SOEC is the safety of hydrogen.

### *6.2. Carbon assisted water electrolysis*

Carbon assisted water electrolysis (CAWE) for hydrogen production was suggested by Coughlin and Farooque 30 years ago [127]. In acidic

electrolyte, hydrogen is still produced on cathode, as shown in Eq. (5). The Eq. (6) for anode reaction is replaced by Eq. (19):

Anode reaction

$$C+2H_2O(l)\rightarrow CO_2(g)+4H^++4e^- \qquad E^\theta=0.21\ \mathrm{V} \tag{19}$$

Total reaction

$$C+2H_2O(l)\rightarrow CO_2(g)+2H_2(g) \qquad U^\theta=0.21\ \mathrm{V} \tag{20}$$

Compared to conventional water electrolysis, carbon is oxidized to $CO_2$ on anode instead of oxygen evolution reaction. For conventional water electrolysis, theoretical decomposition voltage of water is 1.23 V according to Eq. (9) and energy consumption for hydrogen production is 237.2 kJ mol$^{-1}$. For CAWE, theoretical decomposition voltage and energy consumption are only 0.21 V and 40.2 kJ mol$^{-1}$, respectively. Considering reaction overpotential and ohmic voltage drop, initial decomposition voltage of water is usually higher than 0.45 V [128,129]. Generally, carbon sources for anodic reaction are graphite, activated carbon and coal. Coughlin and Farooque [127–129] found that real operating voltage was 0.8–1.0 V for practical hydrogen production using coal as carbon source. That is, actual energy consumption of CAWE is only 1/3 to 1/2 of the energy for conventional water electrolysis. Apparently, the cost for hydrogen production is reduced. However, the composition and structure of coal are very complicated. Besides C element, S, O, N and metal elements (M) also exist abundantly in various forms such as 3OH, –COOH, -S-, -NH-, $MO_x$, $MS_y$ and so on [130–133]. Anodic reactions are mixing reaction during electrolysis. Various functional groups are oxidized easily on anode. However, it is difficult for long carbon chain and benzene rings in coal to be oxidized. Therefore, the reactivity of carbon is restricted. Standard equilibrium anode potential of coal assisted water electrolysis is undeterminable. Energy consumption of coal assisted water electrolysis depends on electrochemical oxidation rate of coal. Coughlin and Farooque [127] found that oxidation rate of coal increased with the increase of coal slurry concentration and temperature in $H_2SO_4$ solution. Patil et al. [134] examined the electrocatalytic activities of various noble metal electrodes for coal oxidation (Fig. 20). Pt–Ir (80:20) electrode was the best anode materials and the maximum faradic efficiency was 24% for $CO_2$ generation. Energy consumption of hydrogen production was 21 W h g$^{-1}$. Yin et al. [135] used Ti-supported metal oxides as anode materials. The results indicated that Ti/$IrO_2$ with $Fe^{3+}$ liquid catalyst exhibited the best catalytic effect on coal oxidation and anode products were mainly $CO_2$ and a spot of alkanes and olefins. An interesting choice is partial electrochemical oxidation of coal on anode to produce valuable small molecular compounds. In this way, the emission of $CO_2$, greenhouse gas, is avoided. Meanwhile, better economy for coal assisted water electrolysis is achieved based on the production of hydrogen on cathode and hydrocarbon organic products on anode. However, the selective control of coal oxidation to target products is the most difficult problem. Hesenov et al. [136] mixed coal slurry with Fe(II)/Fe(III) ions and stirred overnight (> 12 h), and $CO_2$ was not observed in anode compartment at 40 °C and 1.0 V. However, organic compounds are hardly analyzed quantitatively and qualitatively.

When coal is used as carbon source, some uncertainties may occur due to the complexity of coal structure and types. Pure carbon materials such as activated carbon and graphite are better alternative to coal despite of higher cost. Seehra et al. [137] used a fine activated carbon (GX203) as carbon source for CAWE. The measurable $H_2$ was observed at cell voltage of 0.54 V, but hydrogen evolution rate ($R_H$) was very low. In order to increase hydrogen evolution rate, various carbon materials were tested (Fig. 21). Nanocarbon (BP2000) with high surface area was confirmed as the best carbon material [138]. A ten-fold increase in hydrogen evolution rate was obtained at operating voltage of 1.12 V using BP2000 nanocarbon, compared to carbon GX203. Cell voltage was further reduced to 0.72 V with the addition of $FeSO_4$ liquid catalyst and hydrogen evolution rate was not decreased.

The thermodynamics of CAWE is shown in Fig. 22. Both energy demand ($\Delta G$) and decomposition voltage ($U^\theta$) decrease with increase of temperature. When temperature is higher than 900 K, $\Delta G$ becomes negative value. That is, carbon reacts with $H_2O$ to produce $CO_2$ and $H_2$, spontaneously. A novel method that combines SOEC with CAWE is proposed. In SOEC plant, anode reaction proceeds as following:

$$C+O^{2-}\rightarrow CO_2(g)+4e^- \tag{21}$$

Total reaction is same with Eq. (20). Carbon can be also replaced by hydrocarbon such as coal, natural gas, methanol etc [139]. The reaction process is similar to convectional steam reforming for hydrogen production at higher temperature than 900 K [140]. Special advantages are focused for the novel process, compared to convectional steam reforming. Firstly, $H_2$ in cathode compartment and $CO_2$ in anode compartment are separated by solid electrolyte during reaction process. $H_2$ with high purity is produced in situ. Secondly, when cell is operated at higher temperature than 900 K, it serves as solid oxide galvanic cell (SOGC) during hydrogen production and additional electric power is produced between cathode and anode (Fig. 23).

The thermodynamic and kinetic intensification technologies of water electrolysis for hydrogen production are reviewed based on external field, new electrolyte system, solid oxide electrolytic cell

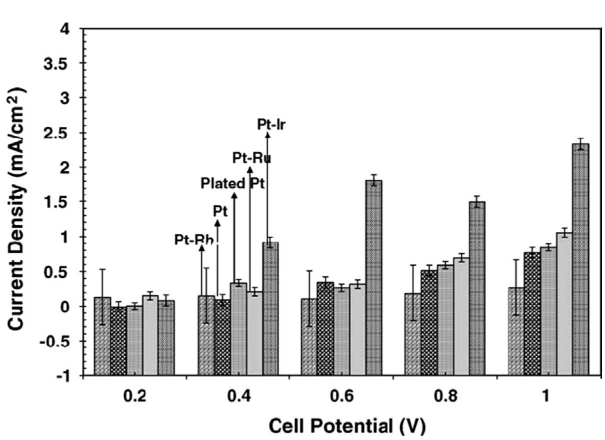



**Fig. 20.** Average current densities on Pt, Pt–Ir, Pt–Ru, Pt–Rh and plated Pt anode for catalytic oxidation of coal slurry with concentration 0.12 g ml$^{-1}$ in 1 M $H_2SO_4$ [134].

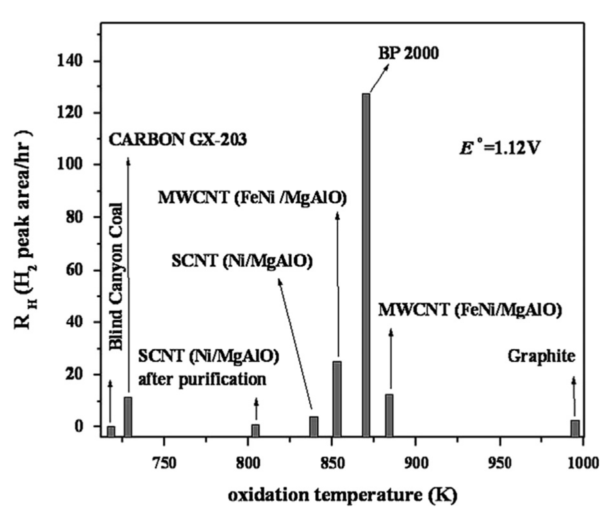



**Fig. 21.** Comparison of hydrogen evolution rate RH measured at 1.12 V for various carbon materials [138].

(SOEC) and carbon assisted water electrolysis (CAWE). A summary and primary comparison of various intensification technologies are given in Fig. 24. Considering cell voltage, the potential of energy saving is more significant for thermodynamic intensification technologies. However, the disadvantages are high operation temperature (SOEC) and enormous change of electrolysis equipments (CAWE). Although cell voltage reduction is relative smaller for kinetic intensification technologies, the operation and application are more simple and flexible. For example, ion activators are added in situ into alkaline electrolyte. No additional cost or equipments are needed.

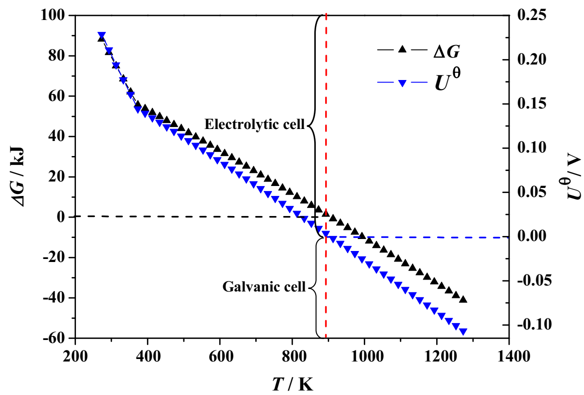



**Fig. 22.** The thermodynamics of carbon assistant water electrolysis at various temperatures.

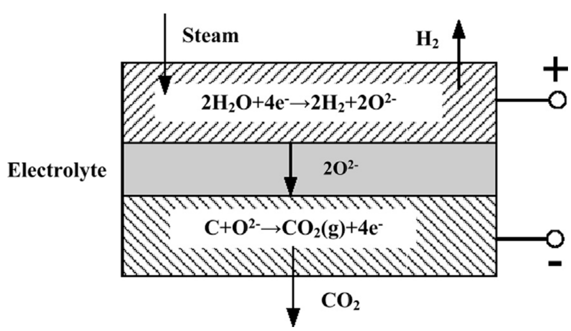



**Fig. 23.** The illustration of solid oxide galvanic cell at temperature higher than 900 K.

## 7. Conclusion

Hydrogen production by water electrolysis coupled with renewable energy is a promising route for the sustainability of energy in future. High energy consumption and cost hinders widespread application of water electrolysis in large scale. The urgent task is to intensify water electrolysis and reduce energy consumption in order to meet the requirement of sustainable hydrogen production.

Considering the kinetics and thermodynamics, process intensification of water electrolysis must be addressed on the main origins of high energy consumption, i.e. theoretical decomposition voltage ($U^\theta$), ohmic voltage drop ($i*\sum R$) and reaction overpotential ($\eta$). During water electrolysis, low interphase separation rate brings about serious bubble effect. Insulating bubbles cover on electrode surface and reduce efficient active area, which leads to high ohmic voltage drop and large reaction overpotential. On the other hand, the dispersion of bubbles in electrolyte also induces high electrolyte resistance. Bubble disengagement from electrolytic system is accelerated by external fields. Particularly, super gravity field exerts directly a driving force on bubbles along buoyancy direction and reduces obviously ohmic voltage drop and reaction overpotential of water electrolysis. The electrocatalytic activity and stability of electrodes are improved by adding ionic activators to electrolyte in situ or using ionic liquid/water electrolyte. Thermodymic decomposition voltage of water is reduced by elevating electrolytic temperature (i.e. SOEC) or changing anode reaction (i.e. CAWE). Interestingly, the combination of SOEC and CAWE provides a novel route to produce pure hydrogen and electricity at higher temperature than 900 K, simultaneously.

The kinetic and thermodynamic process intensification provides instructive opportunities to produce hydrogen by water electrolysis with lower energy consumption. However, the energy to drive external field or elevate temperature of steam need to

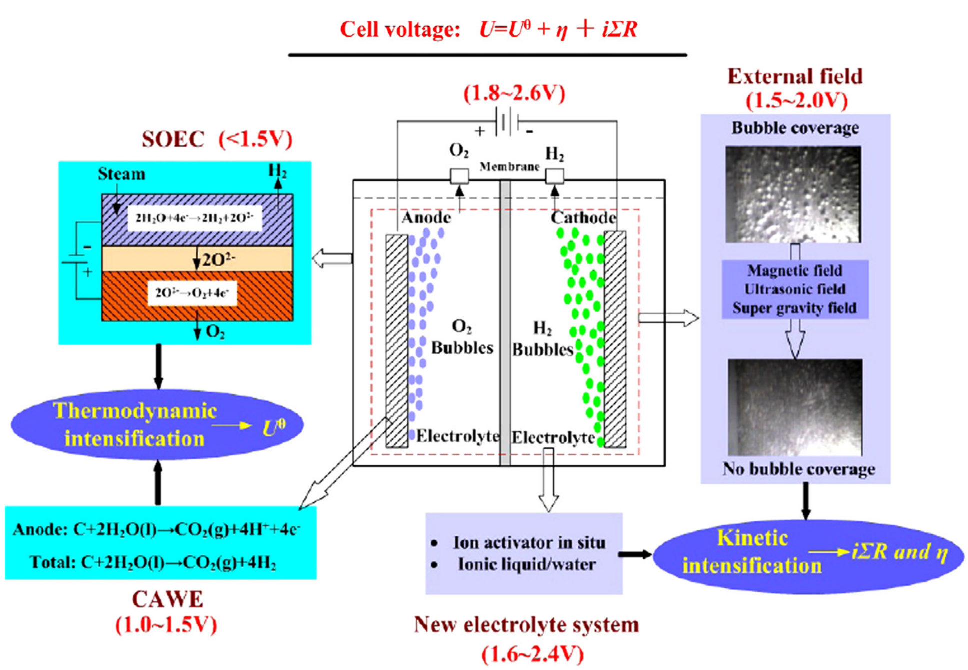



**Fig. 24.** The summary and comparison of intensification technologies to water electrolysis.

be considered. The insight into the intensified mechanism of new technologies on water electrolysis will be further analyzed and discussed. For industrial application, besides process optimization of new technologies, the equipments and process design must be also regarded.

## Acknowledgments

This work is supported by the Natural Science Foundation of China under the Grant 51274180, 51004090 and 50804043.

## References

[1] Balat M. Potential important of hydrogen as a future solution to environmental and transportation problems. International Journal of Hydrogen Energy 2008;33:4013–29.
[2] Ball M, Wietschel M. The future of hydrogen-opportunities and challenges. International Journal of Hydrogen Energy 2009;34:615–27.
[3] Hollada JD, King DL, Wang Y. An overview of hydrogen production technologies. Catalysis Today 2009;139:244–60.
[4] Damyanova S, Pawelec B, Arishtirova K, Fierro JLG. Ni-based catalysts for reforming of methane with $CO_2$. International Journal of Hydrogen Energy 2012;37:15966–75.
[5] Springer TE, Rockward T, Zawodzinski TA, Gottesfeld S. Model for polymer electrolyte fuel cell operation on reformate feed effects of CO, $H_2$ dilution, and high fuel utilization. Journal of The Electrochemical Society 2001;48:A11–23.
[6] Ralph RR, Hogarth MP. Catalysis for low temperature fuel cells. Platinum Metals Review 2002;46:117–35.
[7] Cheng X, Shi Z, Glass N, Zhang L, Zhang J, Song D, et al. A review of PEM hydrogen fuel cell contamination: impacts, mechanisms, and mitigation. Journal of Power Sources 2007;165:739–56.
[8] Reshetenko TV, Bethune K, Rocheleau R. Spatial proton exchange membrane fuel cell performance under carbon monoxide poisoning at a low concentration using a segmented cell system. Journal of Power Sources 2012;218:412–23.
[9] Gosavi PV, Biniwale RB. Catalytic preferential oxidation of carbon monoxide over platinum supported on lanthanum ferrite-ceria catalysts for cleaning of hydrogen. Journal of Power Sources 2013;222:1–9.
[10] Leroy RL. Industrial water electrolysis-present and future. International Journal of Hydrogen Energy 1983;8:401–17.
[11] Sherif SA, Barbir F, Veziroglu TN. Wind energy and the hydrogen economy-review of the technology. Solar Energy 2005;78:647–60.
[12] Palumbo R, Diver RB, Larson C, Voker EN, Miller JE, Guertin J, et al. Solar thermal decoupled water electrolysis process I: proof of concept. Chemical Engineering Science 2012;84:372–80.
[13] Colak I, Sagiroglu S, Yesilbudak M. Data mining and wind power prediction: a literature review. Renewable Energy 2012;46:241–7.
[14] Benli H. Potential of renewable energy in electrical energy production and sustainable energy development of Turkey: performance and polices. Renewable Energy 2013;50:33–46.
[15] Swift-Hook D. Wind energy really is the last to be stored and solar energy cannot be stored economically. Renewable Energy 2013;50:971–6.
[16] Cong RG. An optimization model for renewable energy generation and its application in China: a perspective of maximum utilization. Renewable & Sustainable Energy Reviews 2013;17:94–103.
[17] Djafour A, Matoug M, Bouras H, Bouchekima B, Aida MS, Azoui B. Photovoltaic-assisted alkaline water electrolysis: basic principles. International Journal of Hydrogen Energy 2011;36:4117–24.
[18] Gandia LM, Oroz R, Ursua A, Sanchis P, Dieguez PM. Renewable hydrogen production: performance of an alkaline water electrolyzer working under emulated wind conditions. Energy & Fuels 2007;21:1699–706.
[19] Barbir F. PEM electrolysis for production of hydrogen from renewable energy sources. Solar Energy 2005;78:661–9.
[20] Experimental wind to hydrogen system up and running, 〈http://www.physorg.com/news87494328.html〉.
[21] Yi Y, Lee JK, Uhm S, Nam SC, Lee J. A single-step approach to create nano-pottery structures for efficient water electrocatalysis. Electrochemistry Communications 2009;11:2121–4.
[22] Björketun ME, Bondarenko AS, Abrams BL, Chorkendorff I, Rossmeisl J. Screening of electrocatalytic materials for hydrogen evolution. Physical Chemistry Chemical Physics 2010;12:10536–41.
[23] Laursen AB, Kegnæs S, Dahl S, Chorkendorff I. Molybdenum sulfides-efficient and viable materials for electro-and photoelectrocatalytic hydrogen evolution. Energy and Environmental Science 2012;5:5577–91.
[24] Kibler LA. Hydrogen electrocatalysis. ChemPhysChem 2006;7:985–91.
[25] Liu X, Wang FY. Transition metal complexes that catalyze oxygen formation from water: 1979–2010. Coordination Chemistry Reviews 2012;256:1115–36.
[26] Wang TY, Liu L, Zhu ZW, Papakonstantinou P, Hu JB, Liu HY, et al. Enhanced electrocatalytic activity for hydrogen evolution reaction from self-assembled monodispersed molybdenum sulfide nanoparticles on an Au electrode. Energy and Environmental Science 2013;6:625–33.
[27] Park S, Shao YY, Liu J, Wang Y. Oxygen electrocatalysts for water electrolyzers and reversible fuel cells: status and perspective. Energy and Environmental Science 2012;5:9331–44.
[28] Merrill MD, Dougherty RC. Metal oxide catalysts for the evolution of $O_2$ from $H_2O$. Journal of Physical Chemistry C 2008;112:3655–66.
[29] Damian A, Omanovic S. Ni and Ni–Mo hydrogen evolution electrocatalysts electrodeposited in a polyaniline matrix. Journal of Power Sources 2006 464–76.
[30] Ahn SH, Hwang SJ, Yoo SJ, Choi I, Kim HJ, Jang JH, et al. Electrodeposited Ni dendrites with high activity and durability for hydrogen evolution reaction in alkaline water electrolysis. Journal of Materials Chemistry 2012;22:15153–9.
[31] Lee JK, Yi Y, Lee HJ, Uhm S, Lee J. Electrocatalytic activity of Ni nanowires prepared by galvanic electrodeposition for hydrogen evolution reaction. Catalysis Today 2009;146:188–91.
[32] Wang MY, Wang Z, Guo ZC, Li ZJ. The enhanced electrocatalytic activity and stability of NiW films electrodeposited under super gravity field for hydrogen evolution reaction. International Journal of Hydrogen Energy 2011;36:3305–12.
[33] Mihailov L, Spassov T, Bojinov M. Effect of microstructure on the electrocatalytic activity for hydrogen evolution of amorphous and nanocrystalline Zr–Ni alloys. International Journal of Hydrogen Energy 2012;37:10499–506.
[34] Han Q, Cui S, Pu N, Chen J, Liu K, Wei X. A study on pulse plating amorphous Ni–Mo alloy coating used as HER cathode in alkaline medium. International Journal of Hydrogen Energy 2010;35:5194–201.
[35] Herraiz-Cardona I, Ortega E, Anton JG, Perez-Herranz V. Assessment of the roughness factor effect and the intrinsic catalytic activity for hydrogen evolution reaction on Ni-based electrodeposits. International Journal of Hydrogen Energy 2011;36:9428–38.
[36] Janssen LJJ. Effective solution resistivity in beds containing one monolayer or multilayers of uniform spherical glass beads. Journal of Applied Electrochemistry 2000;30:507–9.
[37] Kiuchi D, Matsushima H, Fukunaka Y, Kuribayashi K. Ohmic resistance measurement of bubble Froth layer in water electrolysis under microgravity. Journal of The Electrochemical Society 2006;153:E138–43.
[38] Aldas K. Application of a two-phase flow model for hydrogen evolution in an electrochemical cell. Applied Mathematics and Computation 2004;154:507–19.
[39] Matsushima H, Fukunaka Y, Kuribayashi K. Water electrolysis under microgravity Part II: description of gas bubble evolution phenomena. Electrochimica Acta 2006;51:4190–8.
[40] Krenz M. Untersuchung des elektrodennahen Raumes gasentwickelnder Elektroden. Dissertation A, Humboldt-Universitat: Berlin; 1984.
[41] Balzer RJ, Vogt H. Effect of electrolyte flow on the bubble coverage of vertical gas-evolving electrodes. Journal of the Electrochemical Society 2003;150:E11–6.
[42] Dukovic J, Tobias CW. The influence of attached bubbles on potential drop and current distribution at gas-evolving electrodes. Journal of the Electrochemical Society 1987;134:331–43.
[43] Ramshaw C. The opportunities for exploiting centrifugal fields. Heat Recovery Systems and CHP 1993;13:493–513.
[44] Qian K, Chen ZD, Chen JJ. Bubble coverage and bubble resistance using cells with horizontal electrode. Journal of Applied Electrochemistry 1998;28:1141–5.
[45] Aldas K, Pehlivanoglu N, Mat MD. Numerical and experimental investigation of two-phase flow in an electrochemical cell. International Journal of Hydrogen Energy 2008;33:3668–75.
[46] Matsushima H, Iida T, Fukunaka Y. Observe of bubble layer formed on hydrogen and oxygen gas-evolving electrode in a magnetic field. Journal of Solid State Electrochemistry 2012;16:617–23.
[47] De La Rue RE, Tobias CW. On the conductivity of dispersions. Journal of the Electrochemical Society 1959;106:827–33.
[48] Mandin P, Aissa AA, Roustan H, Hamburger J, Picard G. Two-phase electrolysis process: from the bubble to the electrochemical cell properties. Chemical Engineering and Processing 2008;47:1926–32.
[49] Janssen LJ. Effective solution resistivity in beds containing one monolayer or multilayers of uniform spherical glass beads. Journal of Applied Electrochemistry 2000;30:507–9.
[50] Li SD, Wang CC, Chen CY. Water electrolysis in the presence of an ultrasonic field. Electrochimica Acta 2009;54:3877–83.
[51] Eigeldinger J, Vogt H. The bubble coverage of gas-evolving electrodes in a flowing electrolyte. Electrochimica Acta 2000;45:4449–56.
[52] Zhang D, Zeng K. Evaluating the behavior of electrolytic gas bubbles and their effect on the cell voltage in alkaline water electrolysis. Industrial & Engineering Chemistry Research 2012;51:13825–32.
[53] Matsushima H, Nohira T, Mogi I, Ito Y. Effects of magnetic fields on iron electrodeposition. Surface and Coatings Technology 2004;179:245–51.
[54] Fernández D, Diao Z, Dunne P, Coev JMD. Influence of magnetic field on hydrogen reduction and co-reduction in the $Cu/CuSO_4$ system. Electrochimica Acta 2010;55:8664–72.
[55] Peipmann R, Lange R, Kubeil C, Mutschke G, Bund A. Magnetic field effects on the mass transport at small electrodes studied by voltammetry and magnetohydrodynamic impedance measurements. Electrochimica Acta 2010;56:133–8.
[56] Iida T, Matsushima H, Fukunaka YJ. Water electrolysis under a magnetic field. Electrochemical Society 2007;154:E112–5.
[57] Lin MY, Hourng LW, Kuo CW. The effect of magnetic force on hydrogen production efficiency in water electrolysis. International Journal of Hydrogen Energy 2012;37:1311–20.
[58] Matsushima H, Kiuchi D, Fukunaka Y. Measurement of dissolved hydrogen supersaturation during water electrolysis in a magnetic field. Electrochemica Acta 2009;54:5858–62.

[59] Koza JA, Uhlemann M, Gebert A, Schultz L. Desorption of hydrogen from the electrode surface under influence of an external magnetic field. Electrochemistry Communications 2008;10:1330–3.
[60] Matsushima H, Iida, Fukunaka Y. Gas bubble evolution on transparent electrode during water electrolysis in a magnetic field. Electrochimica Acta 2013;100:261–4.
[61] Koza JA, Mühlenhoff S, Zabiński P, Nikrityuk PA, Eckert K, Uhlemann M, et al. Hydrogen evolution under the influence of a magnetic field. Electrochimica Acta 2011;56:2665–75.
[62] Hung CY, Li SD, Wang CC, Chen CY. Influences of a bipolar membrane and an ultrasonic field on alkaline water electrolysis. Journal of Membrane Science 2012;389:197–204.
[63] Anlauf H. Recent developments in centrifuge technology. Separation and Purification Technology 2007;58:242–6.
[64] Fagan JA, Becker ML, Chun J, Hobbie EK. Length fractionation of carbon nanotubes using centrifugation. Advanced Materials 2008;20:1609–13.
[65] Zhao LX, Guo ZC, Wang Z, Wang MY. Removal of low-content impurities from Al by super-gravity. Metallurgical and Materials Transactions B 2010;41:505–8.
[66] Li JW, Guo ZC, Tang HQ, Wang Z, Sun ST. Si purification by solidification of Al–Si melt with super gravity. Transactions of Nonferrous Metals Society of China 2012;22:958–63.
[67] Lin SW, Navarro RMF. Effect of centrifugal force on electrodeposition of $Hg^{2+}$ and $Pb^{2+}$ at a spinning graphite electrode. Journal of the Electrochemical Society 2001;148:C284–8.
[68] Cheng H, Scott K, Ramshaw C. Chlorine evolution in a centrifugal field. Journal of Applied Electrochemistry 2002;32:831–8.
[69] Sato M, Yamada A, Aogaki R. Electrochemical reaction in a high gravity field vertical to an electrode surface-analysis of diffusion process with a gravity electrode. Japanese Journal of Applied Physics 2003;42:4320–8.
[70] Atobe M, Murotani A, Hitose S, Suda Y, Sekido M, Fuchigami T, et al. Anodic polymerization of aromatic compounds in centrifugal fields. Electrochimica Acta 2004;50:977–84.
[71] Cheng H, Scott K. Improvement in methanol oxidation in a centrifugal field. Journal of Power Sources 2003;123:137–50.
[72] Mandin P, Cense JM, Georges B, Favre V, Pauporté T, Fukunaka Y, et al. Prediction of the electrodeposition process behavior with the gravity or acceleration value at continuous and discrete scale. Electrochimica Acta 2007;53:233–44.
[73] Wang MY, Wang Z, Guo ZC. Preparation of electrolytic copper powders with high current efficiency enhanced by super gravity field and its mechanism. Transactions of Nonferrous Metals Society of China 2010;20:1154–60.
[74] Lao L, Ramshaw C, Yeung H. Process intensification: water electrolysis in a centrifugal acceleration field. Journal of Applied Electrochemistry 2011;41: 645–56.
[75] Cheng H, Scott K, Ramshaw C. Intensification of water electrolysis in a centrifugal field. Journal of the Electrochemical Society 2002;149:D172–7.
[76] Wang MY, Wang Z, Guo ZC. Water electrolysis enhanced by super gravity field for hydrogen production. International Journal of Hydrogen Energy 2010;35:3198–205.
[77] Wang MY, Wang Z, Guo ZC. Understanding of the intensified effect of super gravity on hydrogen evolution reaction. International Journal of Hydrogen Energy 2009;34:5311–7.
[78] Mat MD, Aldas K. Application of a two-phase flow modal for natural convection in an electrochemical cell. International Journal of Hydrogen Energy 2005;30:411–20.
[79] Kaninski MPM, Maksic AD, Stojic DL, Miljanic SS. Ionic activators in the electrolytic production of hydrogen-cost reduction-analysis of the cathode. Journal of Power Sources 2004;131:107–11.
[80] Kaninski MPM, Nikolic VM, Potkonjak TN, Simonovic BR, Potkonjak NI. Catalytic activity of Pt-based intermetallics for the hydrogen production-Influence of ionic activator. Applied Catalysis A: General 2007;321:93–9.
[81] Kaninski MPM, Saponjic DP, Nikolic VM, Zugic DL, Tasic GS. Energy consumption and stability of the Ni-Mo electrodes for the alkaline hydrogen production at industrial conditions. International Journal of Hydrogen Energy 2011;36:8864–8.
[82] Maksic AD, Miulovic SM, Nikolic VM, Perovic IM, Kaninski MPM. Energy consumption of the electrolytic hydrogen production using Ni–W based activators – Part I. Applied Catalysis A: General 2011;405:25–8.
[83] Kaninski MPM, Saponjic DP, Perovic IM, Maksic AD, Nikolic VM. Electrochemical characterization of the Ni-W catalyst formed in situ during alkaline electrolytic hydrogen production – Part II. Applied Catalysis A: General 2011;405:29–35.
[84] Stojic D, Marceta MP, Sovilj SP, Miljanic ŠS. Hydrogen generation from water electrolysis-possibilities of energy saving. Journal of Power Sources 2003 315–9.
[85] Nikolic VM, Tasic GS, Maksic AD, Saponjic DP, Miulovic SM, Kaninski MPM. Raising efficiency of hydrogen generation from alkaline water electrolysis – energy saving. International Journal of Hydrogen Energy 2010;35:12369–73.
[86] Tasic GS, Maslovara SP, Zugic DL, Maksic AD. Characterization of the Ni–Mo catalyst formed in situ during hydrogen generation from alkaline water electrolysis. International Journal of Hydrogen Energy 2011;36:11588–95.
[87] Wei ZD, Ji MB, Chen SG, Liu Y, Sun CX, Yin GZ, et al. Water electrolysis on carbon electrodes enhanced by surfactant. Electrochimica Acta 2007;52:3323–9.
[88] Rossi A, Boodts JFC. Ir-based oxide electrodes: oxygen evolution reaction from mixed solvent. Journal of Applied Electrochemistry 2002;32:735–41.
[89] Michaud PA, Panizza M, Ouattara L, Diaco T, Foti G, Comninellis C. Electrochemical oxidation of water on synthetic boron-doped diamond thin alloy anodes. Journal of Applied Electrochemistry 2003;33:151–4.
[90] Souza RF, Padukga HC, Goncalves RS, Rault-Berthelot J. Dialkylimidazolium ionic liquids as electrolytes for hydrogen production from water electrolysis. Electrochemistry Communications 2006;8:211–6.
[91] Meang Y, Aldous L, Belding SR, Compton RG. The hydrogen evolution reaction in a room temperature ionic liquid: mechanism and electrocatalyst trends. Physical Chemistry Chemical Physics 2012;14:5222–8.
[92] Souza RF, Padilha JC, Goncalves RS, Souza MO, Rault-Berthelot J. Electrochemical hydrogen production from water electrolysis using ionic liquid as electrolytes: towards the best device. Journal of Power Sources 2007;164:792–8.
[93] Souza RF, Loget G, Padilha JC, Martini EMA, Souza MO. Molybdenum electrodes for hydrogen production by water electrolysis using ionic liquid electrolytes. Electrochemistry Communications 2008;10:1673–5.
[94] Pool DH, Stewart MP, O'Hagan M, Shaw WJ, Roberts JAS, Bullock RM, et al. Acidic ionic liquid/water solution as both medium and proton source for electrocatalytic $H_2$ evolution by $[Ni(P_2N_2)_2]^{2+}$ complexes. Proceedings of the National Academy of Sciences 2012;109:15634–9.
[95] Zeng K, Zhang DK. Recent progress in alkaline water electrolysis for hydrogen production and applications. Progress in Energy and Combustion 2010;36:307–26.
[96] Hauch A, Ebbesen SD, Jensen SH, Mogensen M. Highly efficient high temperature electrolysis. Journal of Materials Chemistry 2008;18:2331–40.
[97] Jiang YZ, Gao JF, Liu MF, Wang YY, Meng GY. Fabrication and characterization of $Y_2O_3$ stabilized $ZrO_2$ films deposited with aerosol-assisted MOCVD. Solid State Ionics 2007;177:3405–10.
[98] Yu B, Zhang WQ, Xu JM, Chen J, Luo X, Stephan K. Preparation and electrochemical behavior of dense YSZ film for SOEC. International Journal of Hydrogen Energy 2012;37:12074–80.
[99] Etsell TH, Flengas SN. Electrical properties of solid oxide electrolytes. Chemical Reviews 1970;70:339–76.
[100] Badwal SPS, Ciacchi FT, Milosevic D. Scandia-zirconia electrolytes for intermediate temperature solid oxide fuel cell operation. Solid State Ionics 2000;136–137:91–9.
[101] Hirano M, Inagaki M, Mizutani Y, Nomura K, Kawai M, Nakamura Y. Mechanical and electrical properties of $Sc_2O_3$-doped zirconia ceramics improved by postsintering with HIP. Solid State Ionics 2000;133:1–9.
[102] Zhu B, Albinsson I, Anderson C, Borsand K, Nilsson M, Mellander BE. Electrolysis studies based on ceria-based composites. Electrochemistry Communications 2006;8:495–8.
[103] Hong HS, Chae US, Choo ST, Lee KS. Microstructure and electrical conductivity of Ni/YSZ and NiO/YSZ composites for high-temperature electrolysis prepared by mechanical alloying. Journal of Power Sources 2005;149:84–9.
[104] O'Brien JE, Stoots CM, Herring JS, Lessing PA, Hartvigsen JJ, Elangovan S. Performance measurements of solid oxide electrolysis cells for hydrogen production. Journal of Fuel Cell Science and Technology 2005;2:156–63.
[105] Hong HS, Chae US, Choo ST. The effect of ball milling parameters and Ni concentration on a YSZ-coated Ni composite for a high temperature electrolysis cathode. Journal of Alloys and Compounds 2008;449:331–4.
[106] Ebbesen SD, Høgh J, Nielsen KA, Nielsen JU, Mogensen M. Durable SOC stacks for production of hydrogen and synthesis gas by high temperature electrolysis. International Journal of Hydrogen Energy 2011;36:7363–73.
[107] Osada N, Uchida H, Watanabe M. Polarization behavior of SDC cathode with highly dispersed Ni catalysts for solid oxide electrolysis cells. Journal of the Electrochemical Society 2006;153:A816–20.
[108] Marina OA, Pederson LR, Williams MC, Coffey GW, Meinhardt KD, Nguyen CD, et al. Electrode performance in reversible solid oxide fuel cells. Journal of the Electrochemical Society 2007;154:B452–9.
[109] Yang X, Irvine JTS. (La0.75Sr0.25)095Mn0.5Cr0.5O3 as the cathode of solid oxide electrolysis cells for high temperature hydrogen production from steam. Journal of Materials Chemistry 2008;18:2349–54.
[110] Liang M, Yu B, Wen M, Chen J, Xu J, Zhai Y. Preparation of LSM-YSZ composite powder for anode of solid oxide electrolysis cell and its activation mechanism. Journal of Power Sources 2009;190:341–5.
[111] Hauch A, Ebbesen SD, Jensen SH, Mogensen M. Highly efficient high temperature electrolysis. Journal of Materials Chemistry 2008;18:2331–40.
[112] Chen KF, Ai N, Jiang SP. Enhanced electrochemical performance and stability of (La, Sr)$MnO_3$–(Gd, Ce)$O_2$ oxygen electrodes of solid oxide electrolysis cells by palladium infiltration. International Journal of Hydrogen Energy 2012;37:1301–10.
[113] Marina OV, Bagger C, Primdahl S, Mogensen M. A solid oxide fuel cell with a gadolinia-doped ceria anode: preparation and performance. Solid State Ions 1999;123:199–208.
[114] Chauveau F, Mougin J, Bassat JM, Mauvy F, Grenier JC. A new anode material for solid oxide electrolyter: the neodymium nickelate $Nd_2NiO_{4+\gamma}$. Journal of Power Sources 2010;195:744–9.
[115] Chauveau F, Mougin J, Mauvy F, Bassat JM, Grenier JC. Development and operation of alternative oxygen electrode materials for hydrogen production by high temperature steam electrolysis. International Journal of Hydrogen Energy 2011;36:7785–90.
[116] Ni M, Leung MKH, Leung DYC. Technological development of hydrogen production by solid oxide electrolyzer cell (SOEC). International Journal of Hydrogen Energy 2008;33:2337–54.
[117] Laguna-Bercero MA. Recent advances in high temperature electrolysis using solid oxide fuel cells: a review. Journal of Power Sources 2012;203:4–16.

[118] Hino R, Haga K, Aita H, Sekita K. R&D on hydrogen production by high-temperature electrolysis of steam. Nuclear Engineering and Design 2004;233:363–75.
[119] Udagawa J, Aguiar P, Brandon NP. Hydrogen production through steam electrolysis: model-based steady state performance of a cathode-supported intermediate temperature solid oxide electrolysis cell. Journal of Power Sources 2007;166:127–36.
[120] Joel MF, Pham AQ, Aceves SM. A natural gas-assisted steam electrolyzer for high-efficiency production of hydrogen. International Journal of Hydrogen Energy 2003;28:483–90.
[121] Yildiz B, Kazimi MS. Efficiency of hydrogen production systems using alternative nuclear energy technologies. International Journal of Hydrogen Energy 2006;31:77–92.
[122] Zhang WQ, Yu B, Xu JM. Efficiency evaluation of high-temperature steam electrolytic systems couple with different nuclear reactors. International Journal of Hydrogen Energy 2012;37:12060–8.
[123] Utgikar V, Thiesen T. Life cycle assessment of high temperature electrolysis for hydrogen production via nuclear energy. International Journal of Hydrogen Energy 2006;31:939–44.
[124] Doenitz W, Schmidberger R, Steinheil E, Streicher R. Hydrogen production by high temperature electrolysis of water vapour. International Journal of Hydrogen Energy 1980;5:55–63.
[125] Ni M, Leung MKH, Leung DYC. Energy and energy analysis of hydrogen production by solid oxide steam electrolyzer plant. International Journal of Hydrogen Energy 2007;32:4648–60.
[126] Sigurvinsson J, Mansilla C, Lovera P, Werkoff F. Can high temperature steam electrolysis function with geothermal heat? International Journal of Hydrogen Energy 2007;32:1174–82.
[127] Coughlin RW, Farooque M. Hydrogen production from coal, water and electrons. Nature 1979;279:301–3.
[128] Coughlin RW, Farooque M. Consideration of electrodes and electrolytes for electrochemical gasification of coal by anodic oxidation. Journal of Applied Electrochemistry 1980;10:729–40.
[129] Coughlin RW, Farooque M. Electrochemical gasification of coal-simultaneous production of hydrogen and carbon dioxide by a single reaction involving coal, water, and electrons. Industrial & Engineering Chemistry Process Design and Development 1980;19:211–9.
[130] Aho MJ, Pirkonen PM. Effects of pressure, gas temperature and $CO_2$ and $O_2$ partial pressures on the conversion of coal-nitrogen to NO, $N_2O$ and $NO_2$. Fuel 1997;74:1677–81.
[131] Yu LE, Hildemann LM, Niksa S. Characteristics of nitrogen-containing aromatic compounds in coal tars during secondary pyrolysis. Fuel 1999;78:377–85.
[132] Zhao W, Yao LP, Lin J, Zong ZM. Electrolytic reduction of Nantong coal and model compounds with oxygenic functional groups in an aqueous NaCl solution. Journal of China University of Mining and Technology 2008;18:112–5.
[133] Chen Y, Mastalerz M, Schimmelmann A. Characterization of chemical functional groups in macerals across different coal ranks via micro-FTIR spectroscopy. International Journal of Coal Geology 2012;104:22–33.
[134] Patil P, Abreu YD, Botte GG. Electrooxidation of coal slurries on different electrode materials. Journal of Power Sources 2006;158:368–77.
[135] Yin RH, Zhao YG, Lu SY, Wang HM, Cao WM, Fan QB. Electrocatalytic oxidation of coal on Ti-supported metal oxides coupled with liquid catalysts for $H_2$ production. Electrochimica Acta 2009;55:46–51.
[136] Hesenov A, Kinik H, Puli G, Gözmen B, Irmak S, Erbatur O. Electrolysis of coal slurries to produce hydrogen gas: relationship between $CO_2$ and $H_2$ formation. International Journal of Hydrogen Energy 2011;36:5361–8.
[137] Seehra MS, Ranganathan S, Manivannan A. Carbon-assisted water electrolysis: an energy-efficient process to produce pure hydrogen at room temperature. Applied Physics Letters 2007;90:044104 (3 pages).
[138] Seehra MS, Bollineni S. Nancarbon boosts energy-efficient hydrogen production in carbon-assisted water electrolysis. International Journal of Hydrogen Energy 2009;34:6078–84.
[139] Martinez-Frias J, Pham A, Aceves SM. A natural gas-assisted steam electrolyzer for high-efficiency production of hydrogen. International Journal of Hydrogen Energy 2003;28:483–90.
[140] Holladay JD, Hu J, King DL, Wang Y. An overview of hydrogen production technologies. Catalysis Today 2009;139:244–60.